

Analysis of general creeping motion of a sphere inside a cylinder

SUKALYAN BHATTACHARYA¹†, COLUMBIA MISHRA¹ AND SONAL BHATTACHARYA²

¹Department of Mechanical Engineering, Texas Tech University, Lubbock, TX 79409, USA

²Department of Electrical & Computer Engineering, Texas Tech University, Lubbock, TX 79409, USA

(Received 15 February 2008; revised 27 August 2009; accepted 27 August 2009;
first published online 7 December 2009)

In this paper, we develop an efficient procedure to solve for the Stokesian fields around a spherical particle in viscous fluid bounded by a cylindrical confinement. We use our method to comprehensively simulate the general creeping flow involving the particle-conduit system. The calculations are based on the expansion of a vector field in terms of basis functions with separable form. The separable form can be applied to obtain general reflection relations for a vector field at simple surfaces. Such reflection relations enable us to solve the flow equation with specified conditions at different disconnected bodies like the sphere and the cylinder. The main focus of this article is to provide a complete description of the dynamics of a spherical particle in a cylindrical vessel. For this purpose, we consider the motion of a sphere in both quiescent fluid and pressure-driven parabolic flow. Firstly, we determine the force and torque on a translating-rotating particle in quiescent fluid in terms of general friction coefficients. Then we assume an impending parabolic flow, and calculate the force and torque on a fixed sphere as well as the linear and angular velocities of a freely moving particle. The results are presented for different radial positions of the particle and different ratios between the sphere and the cylinder radius. Because of the generality of the procedure, there is no restriction in relative dimensions, particle positions and directions of motion. For the limiting cases of geometric parameters, our results agree with the ones obtained by past researchers using different asymptotic methods.

Key words: colloidal systems, particle/fluid flows, Stokesian dynamics

1. Introduction

Transport of particulate complex fluids through a cylinder is a common phenomenon in biological and industrial systems. Examples include blood flow in blood vessels of living organisms or flow of suspensions through microconduits in microfluidic devices. It is common in fluid-mechanical models to assume the suspended particles as spheres. Hence, for biological and microfluidic applications, it is necessary to analyse the hydrodynamic interactions between a spherical particle and a confining cylindrical surface.

In the past, several theoretical investigations have addressed classical flow problems involving creeping motion of a sphere inside a cylinder. Earlier researchers predominantly focused on axial movement of the sphere. Their theories are primarily based on various approximate perturbative schemes which are only valid for different

† Email address for correspondence: s.bhattacharya@ttu.edu

limiting cases (Cox & Mason 1971). These studies can be classified into three categories accordingly.

The first of these approximate techniques is referred as the method of reflection (Brenner & Happel 1958; Cox & Brenner 1967; Greenstein & Happel 1968; Brenner 1970; Greenstein & Happel 1970). In this method, one initially calculates the scattered flow from the sphere in free space with no cylindrical confinement. A correction field is then subtracted to nullify the non-zero velocity at the cylinder surface in the initial approximation. This ensures the satisfaction of the no-slip condition at the conduit, but creates an error in the boundary condition at the sphere surface. Hence, several similar iterations are subsequently performed for improvement which is only possible when distance between the particle centre and the cylinder is much larger than the sphere radius. Other equivalent regular perturbation schemes (Tozeren 1982, 1983) also have similar restrictions.

When distance between the particle centre and the conduit surface is comparable to the particle radius, the method of reflection cannot be used. Then, in the limit of large ratio between the radii of the cylinder and the sphere, one can approximate the surface of the vessel to be nearly planar (Goldman, Cox & Brenner 1967; O'Neill & Stewartson 1967; Falade & Brenner 1985). This second scheme, however, is not applicable when the cylinder radius is comparable to the cylinder-sphere separation.

Finally, theoretical results are also available for configurations where the particle is very tightly fitted in the conduit (Bungay & Brenner 1973*a,b*). In such cases, one can use lubrication theory based on singular perturbation technique to calculate the hydrodynamic friction or mobility of a sphere closely surrounded by a cylindrical surface.

Neither of the aforementioned analysis is, however, applicable when the sphere radius, the cylinder radius and the separation between surfaces of the sphere and the cylinder are comparable. This is why the existing theories are inadequate in describing various physically interesting phenomena (like cell dynamics in arterioles or microfluidic transports) where all three defining dimensions of the particle-conduit system are of the same order. Also, the past studies were mainly focused on axial motion of the particle. However, in presence of an external field like gravity acting in the cross-sectional plane of the cylinder, the particle can move in the radial and azimuthal directions also. To our knowledge, such complete description of the dynamics in a cylinder-sphere system is still not available. Hence, a more general formulation is required to understand particle dynamics both in arbitrary geometry and under the influence of arbitrary forces.

The issue of generality can be addressed by several numerical techniques like boundary integral (Queguiner & Barthes-Biesel 1997; Pozrikidis 2005), spectral boundary element (Higdon & Muldowney 1995), finite element (Lunsmann *et al.* 1993; Sugihara-Seki 1996; Sugihara-Seki & Skalak 1997; Chiu *et al.* 1998) and molecular dynamics (Sushko & Cieplak 2001; Drazer *et al.* 2005) simulations. However, these well-known methods require a considerable computational cost. Thus, a more efficient algorithm is desirable to study colloidal systems in confinements especially if we want to extend the methodology to explain many-particle interactions.

In this paper, we present a semi-analytical procedure which can be efficiently implemented to solve general creeping flow problems involving spherical particles in cylindrical conduits. Our primary focus is to determine the hydrodynamic interactions between a single-spherical particle and a single-confining cylinder though the technique is general enough to be easily extended to multiparticle systems and annular geometries.

Our solution technique has similarities with Stokesian dynamics simulations (often referred as multipolar expansion) which utilize the solution of Stokes equation in spherical coordinates to solve multiparticle interactions in unbounded space (Durllofsky, Brady & Bossis 1987; Ladd 1988; Felderhof & Jones 1989; Sierou & Brady 2001). The method was extended to analyse colloidal systems in wall-bounded slit pore by combining boundary integral and the spherical solutions (Durllofsky & Brady 1989). The same problem is also approximately solved by modelling the bounding planar walls as closely packed arrays of static spheres so that the free-space many-sphere computation can simply be extended without any further complexity (Nott & Brady 1994; Morris & Brady 1998). More accurate results can be obtained with even less cost, if the spherical solutions are applied in conjunction with proper reflection relations for a single planar wall (Cichocki & Jones 1998; Cichocki *et al.* 2000) or two such walls (Bhattacharya & Bławdziewicz 2002). Recently, the efficiency has been further increased by devising a scheme which analyses many-sphere problem between two planes by using two sets of Stokesian solutions (Bhattacharya, Bławdziewicz & Wajnryb 2005*a,b*, 2006*a,b*; Bhattacharya 2008*a*). Moreover, similar analysis is applied to unsteady flow between planar walls (Bhattacharya 2008*b*), and steady axisymmetric systems (Wang & Skalak 1969). Applicability of this efficient algorithm is, however, restricted to planar wall or axisymmetric geometries due to its crucial dependence on translational or rotational symmetries which are not a necessity for the general formulation outlined in this paper.

The presented method is based on the basis function expansion of a vector field governed by a second-order linear differential equation. For our particular problem, the vector field is the flow field and the second-order governing equation is the Stokes equation. Accordingly, we find complete sets of separable basis solutions for the Stokes equation in cylindrical and spherical coordinates which correspond to the conduit and the particle surface, respectively. The separable solutions are used to find general reflection relations at the respective surfaces so that any prescribed field at the interfaces can be described appropriately. For simultaneous satisfaction of the boundary conditions at both spherical and cylindrical surfaces, proper transformation relations between spherical and cylindrical basis solutions are derived. These transformation relations along with the reflection relations are used to obtain necessary results for arbitrary geometric configurations.

This paper is organized in the following manner. In §2, we describe how we satisfy boundary conditions at disconnected simple surfaces by using separable basis solutions and general reflection relations. In §3, we solve Stokes equation in the presence of a sphere inside a cylinder by following the outlined procedure. Numerical implementation and convergence tests are presented in §4. In §5, we apply our algorithm to find hydrodynamic friction coefficients of the particle translating and rotating in quiescent fluid for arbitrary geometric configurations and arbitrary direction of motion. In the limiting cases, we compare our results with existing data to validate our analysis by showing the relative error to be less than 1%. In §6, we consider the particle to be in a pressure-driven parabolic flow, and determine the hydrodynamic friction when it is fixed as well as the hydrodynamic mobility when it is freely moving. Finally, the conclusions are drawn in §7.

2. Basis transformation method

In this section, we present an outline of the general mathematical procedure (referred as basis transformation method) that is used in our analysis. The key

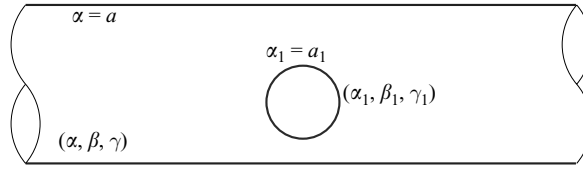


FIGURE 1. The conduit and particle coordinates.

features of this method are similar to simple separation of variables used for solving a linear partial differential equation apart from two crucial differences. Firstly, in our problem the boundary conditions are specified at different kinds of disconnected surfaces (the conduit and the particle). Secondly, these conditions specify a vectorial field (velocity) instead of a scalar which is generally the dependent variable in the separation of variable.

2.1. Geometry and coordinate systems

In the analysis, we assign two different coordinate systems for the conduit and the particle assuming simple enough geometries for both. For a general confinement and a general particle these coordinates are denoted by (α, β, γ) and $(\alpha_1, \beta_1, \gamma_1)$, respectively. Accordingly, the conduit and the particle are described by α -constant and α_1 -constant surfaces. For the particle–fluid interface, we consider $\alpha_1 = a_1$. If the confined domain is bounded by a single surface (as in one-wall or cylindrical geometries), we assume the surface is represented by $\alpha = a$. In contrast, if two isolated boundaries are present (as in two-wall or annular geometries), we define the additional surface by $\alpha = a'$ with $a' < a$. Though our method can be applied for annular and two-wall geometries, at present, we only concentrate on a single-surface conduit which is the case for a cylindrical vessel.

Hence, in our specific problem, (α, β, γ) are the cylindrical coordinates (ρ, β, z) with z axis coinciding with the conduit axis whereas $(\alpha_1, \beta_1, \gamma_1)$ are the spherical coordinates (r, θ, ϕ) with origin at the particle centre. So, according to our notation, the conduit radius is a and the particle radius is a_1 . The specific geometry and coordinates are schematically described in figure 1. It is to be noted that this general procedure also works for other geometries. For example, the conduit coordinates would be Cartesian if the confinement is a planar wall, or the particle coordinate will be spheroidal if the particle is a spheroid.

2.2. Complete set of separable basis solutions

Once the coordinates are assigned, we focus on the expression of general vectorially separable basis solutions for the governing equation in both (α, β, γ) and $(\alpha_1, \beta_1, \gamma_1)$ coordinate systems. As the governing equation is of second order, we need two independent solutions for each system to properly solve the vector field. Accordingly, the separable basis solutions for the conduit and the particle coordinates are denoted as $\mathbf{v}_{\lambda\mu\sigma}^{\pm}$ and $\mathbf{v}_{lm\sigma}^{1\pm}$, respectively. The superscripts $+$ and $-$ represent two different kinds of solutions.

At this point, we provide a detailed description of the subscripts in $\mathbf{v}_{\lambda\mu\sigma}^{\pm}$ and $\mathbf{v}_{lm\sigma}^{1\pm}$ to clarify their meaning. The indices l and m are required to construct a complete set in scalar functional space for the particle coordinates. These are generally discrete numbers like the indices of spherical or spheroidal harmonics in spherical or spheroidal coordinates. Similarly, λ and μ are indices associated with the scalar functional space in (α, β, γ) system. These indices can be either discrete or continuous depending on the confinements. For Stokesian fields near planar walls, λ and μ are the

x and y components of continuous wave vectors whereas for cylindrical geometries λ is the magnitude of continuous wave vector and μ is a discrete number associated with azimuthal dependence as $\exp(i\mu\beta)$. The other index $\sigma = 0, 1, 2$ indicates three independent solutions that complete the set of vectorial basis functions in three-dimensional space.

In order to satisfy arbitrary linear non-homogeneous boundary conditions at the particle and the conduit surface, $\mathbf{v}_{\lambda\mu\sigma}^{\pm}$ and $\mathbf{v}_{lm\sigma}^{\pm}$ have to be in the following form:

$$\mathbf{v}_{\lambda\mu\sigma}^{\pm} = \mathbf{S}(\alpha, \beta, \gamma) \cdot \sum_{s=0,1,2} \mathbf{e}_{\lambda\mu s}(\alpha, \beta, \gamma) f_{\lambda\mu s\sigma}^{\pm}(\alpha) \quad (2.1)$$

and

$$\mathbf{v}_{lm\sigma}^{1\pm} = \mathbf{S}^1(\alpha_1, \beta_1, \gamma_1) \cdot \sum_{s=0,1,2} \mathbf{e}_{lms}^1(\alpha_1, \beta_1, \gamma_1) f_{lms\sigma}^{1\pm}(\alpha_1). \quad (2.2)$$

The index-independent second-order invertible tensorial function \mathbf{S} or \mathbf{S}^1 are identity tensor for the present problem. The index-dependent single-variable scalar functions $f_{\lambda\mu s\sigma}^{\pm}$ s or $f_{lms\sigma}^{1\pm}$ s in (2.1) and (2.2) are to be determined for particular governing equations and coordinate systems. We also impose additional finiteness criteria so that for finite α and α_1 (i) $f_{\lambda\mu s\sigma}^+$ is finite for $\alpha < \infty$, (ii) $f_{\lambda\mu s\sigma}^-$ is finite for $\alpha > 0$, (iii) $f_{lms\sigma}^{1+}$ is finite for $\alpha_1 < \infty$ and (iv) $f_{lms\sigma}^{1-}$ is finite for $\alpha_1 > 0$.

The vectors $\mathbf{e}_{\lambda\mu s}$ or \mathbf{e}_{lms}^1 form a complete set of orthogonal fields in terms of which any vector function can be expanded at α - or α_1 -constant surface, respectively:

$$\int \mathbf{e}_{\lambda\mu s}^* \cdot \mathbf{e}_{\lambda'\mu's'} d\beta d\gamma = \delta_{\lambda\lambda'} \delta_{\mu\mu'} \delta_{ss'} \quad (2.3)$$

and

$$\int \mathbf{e}_{lms}^{1*} \cdot \mathbf{e}_{l'm's'}^1 d\beta_1 d\gamma_1 = \delta_{ll'} \delta_{mm'} \delta_{ss'}, \quad (2.4)$$

where the superscript * denotes complex conjugate and δ is either the Kronecker delta or the Dirac delta function depending on whether the subscripts are discrete or continuous.

The presented method can be applied only when the governing equations and the geometries are such that the vector basis functions can be expressed by (2.1)–(2.4). Fortunately, for common equations like steady or periodically transient Stokes equation and for simple geometries like spherical particle, cylindrical conduit or planar wall, such basis functions can be constructed. In all of these cases, the general solution for the vector field \mathbf{v} can be expressed as a linear combination of either $\mathbf{v}_{\lambda\mu\sigma}^{\pm}$:

$$\mathbf{v} = \sum_{\lambda\mu\sigma} (\mathbf{v}_{\lambda\mu\sigma}^+ b_{\lambda\mu\sigma}^+ + \mathbf{v}_{\lambda\mu\sigma}^- b_{\lambda\mu\sigma}^-) \quad (2.5)$$

or $\mathbf{v}_{lm\sigma}^{1\pm}$:

$$\mathbf{v} = \sum_{lm\sigma} (\mathbf{v}_{lm\sigma}^{1+} c_{lm\sigma}^+ + \mathbf{v}_{lm\sigma}^{1-} c_{lm\sigma}^-), \quad (2.6)$$

where $b_{\lambda\mu\sigma}^{\pm}$ and $c_{lm\sigma}^{\pm}$ are scalar amplitudes, and \sum implies discrete summation for discrete indices and integral for continuous indices. In this analysis, the vector field \mathbf{v} is solved by obtaining the unknown coefficients $c_{lm\sigma}^+$ and $c_{lm\sigma}^-$.

2.3. General reflection relations at the particle and the conduit surface

In the next step, we consider an inhomogeneous boundary condition at the particle surface. We only consider Dirichlet conditions though other linear conditions can also be analysed by this general technique. Accordingly, we assume that the vector field \mathbf{v} at $\alpha_1 = a_1$ is $\mathbf{V}(\beta_1, \gamma_1)$ which is a function of β_1 and γ_1 . We can express $\mathbf{V}(\beta_1, \gamma_1)$ in two different ways. Firstly, considering \mathbf{S}^1 to be identity tensor and set of orthogonal vector functions \mathbf{e}_{lms}^1 to be complete, one can write $\mathbf{V}(\beta_1, \gamma_1)$ as a linear combination:

$$\mathbf{V}(\beta_1, \gamma_1) = \sum_{lms} \mathbf{e}_{lms}^1 a_{lms}, \quad (2.7)$$

where a_{lms} 's are the amplitudes. Secondly, $\mathbf{V}(\beta_1, \gamma_1)$ can also be obtained from the vector field \mathbf{v} in (2.6). By combining (2.2) and (2.6), and by setting $\alpha_1 = a_1$, we determine

$$\mathbf{V}(\beta_1, \gamma_1) = \sum_{lms\sigma} \mathbf{e}_{lms}^1 [f_{lms\sigma}^{1+}(a_1)c_{lms}^+ + f_{lms\sigma}^{1-}(a_1)c_{lms}^-]. \quad (2.8)$$

Hence, by comparing (2.7) and (2.8), one can find a relation between a_{lms} , c_{lms}^+ and c_{lms}^- :

$$\sum_{\sigma} [f_{lms\sigma}^{1-}(a_1)c_{lms}^- + f_{lms\sigma}^{1+}(a_1)c_{lms}^+] = a_{lms}. \quad (2.9)$$

For a given inhomogeneous Dirichlet condition at the particle–fluid interface, a_{lms} is known. As a result, (2.9) serves as one of the constraint equations required for determination of the unknown coefficients c_{lms}^- and c_{lms}^+ .

Apart from (2.9), an additional equation is necessary for evaluation of c_{lms}^- and c_{lms}^+ . This equation is derived from the boundary condition at the conduit where $\mathbf{v} = 0$ for any $\mathbf{V}(\beta_1, \gamma_1)$. To this end, we find two sets of transformation relations between the basis solutions of the particle and the conduit coordinates. For simplicity, we assume only the case where the particle is inside the conduit so that the domain is defined by $\alpha < a$ and $\alpha_1 > a_1$. In this situation, the finiteness criteria for $f_{\lambda\mu\sigma}^{\pm}$ and $f_{lms\sigma}^{1\pm}$ ensure the existence of two transformation relations for given relative position vector \mathbf{R} between the particle and the conduit centres. These transformations are

$$\mathbf{v}_{lms}^{1-}(\mathbf{r}) = \sum_{\lambda\mu\sigma'} \mathbf{v}_{\lambda\mu\sigma'}^-(\mathbf{r}) T_f(\lambda\mu\sigma', lms | \mathbf{R}), \quad (2.10)$$

as long as α_R (the value of α associated with \mathbf{R}) is smaller than α (related to \mathbf{r}), and

$$\mathbf{v}_{\lambda\mu\sigma}^+(\mathbf{r}) = \sum_{lms'} \mathbf{v}_{lms'}^+(\mathbf{r}) T_r(\mathbf{R} | lms', \lambda\mu\sigma), \quad (2.11)$$

where T_f and T_r are the transformation coefficients. By substituting (2.10) in (2.6) and (2.11) in (2.5) and comparing, we determine

$$b_{\lambda\mu\sigma}^- = \sum_{lms'} T_f(\lambda\mu\sigma, lms' | \mathbf{R}) c_{lms'}^- \quad (2.12)$$

and

$$c_{lms}^+ = \sum_{\lambda\mu\sigma'} T_r(\mathbf{R} | lms, \lambda\mu\sigma') b_{\lambda\mu\sigma'}^+. \quad (2.13)$$

Again substituting (2.12) in (2.5) and considering no slip at the conduit, one obtains

$$\mathbf{v}|_{\alpha=a} = 0 = \sum_{\lambda\mu\sigma} \mathbf{e}_{\lambda\mu\sigma} \left[f_{\lambda\mu\sigma}^+(a) b_{\lambda\mu\sigma}^+ + f_{\lambda\mu\sigma}^-(a) \sum_{lms'} T_f(\lambda\mu\sigma, lms' | \mathbf{R}) c_{lms'}^- \right]. \quad (2.14)$$

Hence setting the square bracketed term in (2.14) as zero and using (2.13), we can derive the additional relation between $c_{lm\sigma}^+$ and $c_{lm\sigma}^-$.

This second relation between $c_{lm\sigma}^+$ and $c_{lm\sigma}^-$ can be simplified in terms of the reflection coefficients which ensure the satisfaction of the no-slip boundary condition at the conduit surface. By combining (2.13) and (2.14), one finds

$$c_{lm\sigma}^+ = - \sum_{l'm'\sigma'} \sum_{\lambda\mu\sigma_1\sigma_2} T_r(\mathbf{R} | lm\sigma, \lambda\mu\sigma_1) R_c(\lambda\mu\sigma_1\sigma_2; a) T_f(\lambda\mu\sigma_2, l'm'\sigma' | \mathbf{R}) c_{l'm'\sigma'}^- \quad (2.15)$$

The conduit reflection coefficients R_c can be determined if $f_{\lambda\mu\sigma}^\pm$ s are known

$$R_c(\lambda\mu\sigma_1\sigma_2; a) = \sum_{s=0,1,2} g_{\lambda\mu\sigma_1s}^+(a) f_{\lambda\mu\sigma_2}^-(a), \quad (2.16)$$

where the scalar function $g_{\lambda\mu\sigma_1s}^+(a)$ is such that the following relation can be satisfied

$$\sum_{s=0,1,2} g_{\lambda\mu\sigma_1s}^+(a) f_{\lambda\mu\sigma_2}^+(a) = \delta_{\sigma_1\sigma_2}. \quad (2.17)$$

The existence of $g_{\lambda\mu\sigma_1s}^+$ is assured because of the linear independence of $\mathbf{v}_{\lambda\mu 0}^+$, $\mathbf{v}_{\lambda\mu 1}^+$, $\mathbf{v}_{\lambda\mu 2}^+$.

Finally, (2.9) and (2.15) are combined to calculate the unknown coefficients $c_{lm\sigma}^+$ and $c_{lm\sigma}^-$ so that the Dirichlet boundary condition at both particle and confinement can be satisfied simultaneously. One can eliminate $c_{lm\sigma}^+$ from these equations by using a second type of reflection coefficient R_p which is associated with the particle. Accordingly, after substituting $c_{lm\sigma}^+$ as per (2.15) in (2.9) and defining reflection coefficient R_p properly, we find

$$d_{lm\sigma} = \sum_s g_{lm\sigma s}^{1+}(a_1) a_{lms} = \sum_{\sigma''} R_p(lm\sigma\sigma''; a_1) c_{lm\sigma''}^- - \sum_{l'm'\sigma'} \sum_{\lambda\mu\sigma_1\sigma_2} T_r(\mathbf{R} | lm\sigma, \lambda\mu\sigma_1) R_c(\lambda\mu\sigma_1\sigma_2; a) T_f(\lambda\mu\sigma_2, l'm'\sigma' | \mathbf{R}) c_{l'm'\sigma'}^-, \quad (2.18)$$

where R_p can be expressed in terms of $f_{lm\sigma}^{1\pm}$. The relation between R_p and $f_{lm\sigma}^{1\pm}$ is similar to the relation between R_c and $f_{\lambda\mu\sigma}^\pm$:

$$R_p(lm\sigma\sigma'; a_1) = \sum_{s=0,1,2} g_{lm\sigma s}^{1+}(a_1) f_{lm\sigma'}^{1-}(a_1), \quad (2.19)$$

where

$$\sum_{s=0,1,2} g_{lm\sigma s}^{1+}(a_1) f_{lm\sigma'}^{1+}(a_1) = \delta_{\sigma\sigma'}. \quad (2.20)$$

Hence, for a given boundary condition at the particle where $d_{lm\sigma}$ is known, we first solve (2.18) and then use (2.15) for the complete solution.

In spite of apparent mathematical complexity, the key elements of the method are simple. Firstly, we determine two sets of separable basis solutions and use the four indexed scalar functions to construct the coefficients for particle reflection R_p and confinement reflection R_c . Then two types of transformation coefficients denoted by T_f and T_r are evaluated. Finally, we solve the vector field \mathbf{v} by calculating the amplitudes $c_{lm\sigma}^-$ and $c_{lm\sigma}^+$ from (2.18) and (2.15), respectively. In order to keep the analysis simple, in this paper we specifically assume that (i) boundary conditions are Dirichlet, (ii) a single surface forms the confinement, (iii) the particle is inside the

vessel and (iv) only a single particle is present in the system. Fortunately, with minor modifications, the technique can also be applied to a far more general scenario where all these assumptions are relaxed.

3. General Stokesian solution for flow around a sphere in a cylinder

To analyse creeping motion of a spherical particle inside a cylindrical vessel, we treat Stokes equation as the second-order vector equation mentioned in §2:

$$\eta \nabla^2 \mathbf{v} = \nabla p \quad \nabla \cdot \mathbf{v} = 0. \quad (3.1)$$

Here, η is viscosity, \mathbf{v} is velocity-field and p is pressure. The Dirichlet conditions are specified at the surfaces of the sphere and the cylinder where \mathbf{v} is known.

In the analysis, the particle coordinate system $(\alpha_1, \beta_1, \gamma_1)$ is denoted by spherical coordinates (r, θ, ϕ) whereas conduit coordinate system (α, β, γ) is represented by cylindrical coordinates (ρ, β, z) . Following the outlined procedure, we find separable basis velocities for Stokes equation in cylindrical and spherical coordinates according to (2.1) and (2.2), and calculate R_c and R_p . Then, we show how to derive corresponding T_f and T_r .

The analysis can be drastically simplified if one takes advantage of two well-known symmetries. In the next two subsections, we show how to use these two symmetries.

3.1. The recurrence curl relation between the basis solutions of Stokes equation

Using vector identities, the Stokes equation (3.1) can be rewritten in an equivalent form

$$\nabla \times \nabla \times \nabla \times \mathbf{v} = 0. \quad (3.2)$$

From the recurrence of the operator $\nabla \times$ in (3.2), one can draw the following conclusion about the solutions of Stokes equation: if one finds a solution \mathbf{v}_{prs} for which $\nabla \times \nabla \times \mathbf{v}_{prs}$ is non-trivial, then $\mathbf{v}_{vor} = q \nabla \times \mathbf{v}_{prs}$ and $\mathbf{v}_{pot} = q \nabla \times \mathbf{v}_{vor}$ (with q being a constant) are also two independent solutions. This recurrence symmetry of Stokesian fields is well known (Bhattacharya *et al.* 2005a,b) and \mathbf{v}_{prs} , \mathbf{v}_{vor} , \mathbf{v}_{pot} are similar to the pressure, vorticity and potential solutions described in (Lamb 1945). This recurrence symmetry has a twofold advantage.

Firstly, due to the recurrence relation, the construction of the basis solutions becomes easier – we do not need to derive individually all three solutions corresponding to $\sigma = 0, 1, 2$. We obtain only that one which gives non-trivial field when operated on twice by the Curl operator and assign one value of σ for the solution. The other two basis fields corresponding to the other two values of σ are derived by taking Curl and double Curl of the first solution. Accordingly, we follow the convention where $\mathbf{v}_{\lambda\mu 2}^+$, $\mathbf{v}_{\lambda\mu 0}^-$, $\mathbf{v}_{lm 2}^+$ and $\mathbf{v}_{lm 0}^-$ have non-trivial double Curl and

$$\mathbf{v}_{\lambda\mu 1}^- = q^- \nabla \times \mathbf{v}_{\lambda\mu 0}^-, \quad \mathbf{v}_{\lambda\mu 2}^- = q^- \nabla \times \mathbf{v}_{\lambda\mu 1}^-, \quad (3.3)$$

$$\mathbf{v}_{\lambda\mu 1}^+ = q^+ \nabla \times \mathbf{v}_{\lambda\mu 2}^+, \quad \mathbf{v}_{\lambda\mu 0}^+ = q^+ \nabla \times \mathbf{v}_{\lambda\mu 1}^+, \quad (3.4)$$

$$\mathbf{v}_{lm 1}^- = q_1^- \nabla \times \mathbf{v}_{lm 0}^-, \quad \mathbf{v}_{lm 2}^- = q_1^- \nabla \times \mathbf{v}_{lm 1}^-, \quad (3.5)$$

$$\mathbf{v}_{lm 1}^+ = q_1^+ \nabla \times \mathbf{v}_{lm 2}^+, \quad \mathbf{v}_{lm 0}^+ = q_1^+ \nabla \times \mathbf{v}_{lm 1}^+, \quad (3.6)$$

where q^\pm , q_1^\pm are four constants which are chosen as per convenience. Among the solutions defined in (3.3)–(3.6), the ones with $\sigma = 1$ are solenoidal harmonic vector fields whereas remaining solutions ($\mathbf{v}_{\lambda\mu 2}^-$, $\mathbf{v}_{\lambda\mu 0}^+$, $\mathbf{v}_{lm 2}^-$, $\mathbf{v}_{lm 0}^+$) are potential fields.

The second benefit of the recurrence relation is simplification of the derivation of T_f and T_r . By taking Curl and double Curl of (2.10) and using (3.3) and (3.5), we find

$$T_f(\lambda\mu\sigma' + j, lm\sigma + j) = (q_1^-/q^-)^j T_f(\lambda\mu\sigma', lm\sigma) \quad \text{for } j < 2 - \max(\sigma', \sigma) \quad (3.7)$$

and

$$T_f(\lambda\mu\sigma', lm\sigma) = 0 \quad \text{for } \sigma' < \sigma, \quad (3.8)$$

where ‘max’ means the maximum of the arguments, and \mathbf{R} is omitted for notational simplicity. Hence, T_f for all σ and σ' can be defined by only three coefficients instead of nine – we determine $T_f(\lambda\mu 0, lm 0)$, $T_f(\lambda\mu 1, lm 0)$, $T_f(\lambda\mu 2, lm 0)$ in terms of which the remaining non-zero coefficients can be expressed. Similarly, we can also simplify T_r by taking Curl and double Curl of (2.11) and using (3.4) and (3.6):

$$T_r(lm\sigma + j, \lambda\mu\sigma' + j) = (q_1^+/q^+)^j T_r(lm\sigma, \lambda\mu\sigma') \quad \text{for } j < 2 - \max(\sigma', \sigma) \quad (3.9)$$

and

$$T_r(lm\sigma, \lambda\mu\sigma') = 0 \quad \text{for } \sigma' < \sigma. \quad (3.10)$$

For these coefficients, we evaluate only $T_r(lm 0, \lambda\mu 2)$, $T_r(lm 1, \lambda\mu 2)$, $T_r(lm 2, \lambda\mu 2)$, and utilize (3.9) to find other non-zero coefficients for different σ and σ' .

3.2. Normalization by Oseen tensor

In the previous subsection, it is shown that if somehow we can derive the expressions for Stokesian solutions with non-trivial double Curl (i.e. $\mathbf{v}_{\lambda\mu 2}^+$, $\mathbf{v}_{\lambda\mu 0}^-$, $\mathbf{v}_{lm 2}^+$, $\mathbf{v}_{lm 0}^-$), then we can complete the set of basis fields for different σ very easily. However, there is no unique way to construct the aforementioned fields because of gauge invariance. We can always add irrotational or solenoidal-harmonic vector functions to $\mathbf{v}_{\lambda\mu 2}^+$, $\mathbf{v}_{\lambda\mu 0}^-$, $\mathbf{v}_{lm 2}^+$, $\mathbf{v}_{lm 0}^-$ without contradicting their definitions. In this subsection, we use another symmetry of the Stokesian solutions for unique representation of these basis fields. In the process, we take advantage of the inherent gauge invariance to simplify the subsequent analysis.

Among the Stokesian basis, the ones corresponding to a potential field are the only solutions that are unaffected by the gauge fields. So they can be uniquely defined (besides normalization constants) as gradients of harmonic scalar fields:

$$\mathbf{v}_{\lambda\mu 2}^- = \nabla\Phi_{\lambda\mu}^-, \quad \mathbf{v}_{\lambda\mu 0}^+ = \nabla\Phi_{\lambda\mu}^+, \quad \mathbf{v}_{lm 2}^{1-} = \nabla\Phi_{lm}^{1-}, \quad \mathbf{v}_{lm 0}^{1+} = \nabla\Phi_{lm}^{1+}, \quad (3.11)$$

where $\Phi_{\lambda\mu}^\pm$, $\Phi_{lm}^{1\pm}$ are separable solutions for Laplace equation in respective coordinates

$$\begin{aligned} \Phi_{\lambda\mu}^- &= \frac{K_\mu(\lambda\rho)\mathbf{e}^{i(\mu\beta+\lambda z)}}{A_{\lambda\mu}^-}, & \Phi_{\lambda\mu}^+ &= \frac{I_\mu(\lambda\rho)\mathbf{e}^{i(\mu\beta+\lambda z)}}{A_{\lambda\mu}^+}, & \Phi_{lm}^{1-} &= \frac{Y_{lm}(\theta, \phi)}{A_{lm}^{1-}r^{l+1}}, \\ \Phi_{lm}^{1+} &= \frac{r^l Y_{lm}(\theta, \phi)}{A_{lm}^{1+}}. \end{aligned} \quad (3.12)$$

In (3.12) K_μ and I_μ are two kinds of modified Bessel functions of integer order μ ; Y_{lm} are normalized spherical harmonics, and $A_{\lambda\mu}^\pm$, $A_{lm}^{1\pm}$ are scaling constants. We set

$$A_{\lambda\mu}^- = 4\pi^2/A_{\lambda\mu}^+, \quad A_{lm}^{1-} = (2l + 1)/A_{lm}^{1+}, \quad (3.13)$$

so that the properties of $\Phi_{\lambda\mu}^{\pm}$, $\Phi_{lm}^{1\pm}$ ensure that the Greens function G_r for Laplace equation can be expressed as below:

$$G_r(\mathbf{r} - \mathbf{r}') = \frac{1}{4\pi|\mathbf{r} - \mathbf{r}'|} = \int_{-\infty}^{\infty} \sum_{\mu=-\infty}^{\infty} \Phi_{\lambda\mu}^{+*}(\mathbf{r}') \Phi_{\lambda\mu}^{-}(\mathbf{r}) d\lambda = \sum_{l=1}^{\infty} \sum_{m=-l}^l \Phi_{lm}^{1+*}(\mathbf{r}') \Phi_{lm}^{1-}(\mathbf{r}), \quad (3.14)$$

where \mathbf{r} is position of the observation point and \mathbf{r}' is the position of a source. Two vectors \mathbf{r} and \mathbf{r}' are such that $\rho > \rho'$ and $r > r'$ where primed coordinates relate to \mathbf{r}' .

Using (3.3)–(3.6) and identifying special features of Oseen tensor as described in Appendix A, we find

$$\mathbf{T}(\mathbf{r} - \mathbf{r}') = \frac{1}{8\pi|\mathbf{r} - \mathbf{r}'|} [\mathbf{I} - (\mathbf{r} - \mathbf{r}')(\mathbf{r} - \mathbf{r}')/|\mathbf{r} - \mathbf{r}'|^2], \quad (3.15)$$

it can be shown that

$$\mathbf{T}(\mathbf{r} - \mathbf{r}') = \sum_{\lambda\mu\sigma'} \mathbf{v}_{\lambda\mu\sigma'}^{+*}(\mathbf{r}') \mathbf{v}_{\lambda\mu\sigma'}^{-}(\mathbf{r}) = \sum_{lm\sigma} \mathbf{v}_{lm\sigma}^{1+*}(\mathbf{r}') \mathbf{v}_{lm\sigma}^{1-}(\mathbf{r}), \quad (3.16)$$

when $q^{+*} = q^{-} = q_1^{+*} = q_1^{-} = i$ and $\mathbf{v}_{\lambda\mu 2}^{+}$, $\mathbf{v}_{\lambda\mu 0}^{-}$, $\mathbf{v}_{lm 2}^{1+}$, $\mathbf{v}_{lm 0}^{1-}$ are constructed in a unique way by fixing the gauge fields. We impose the additional constraint described as (3.16) on $\mathbf{v}_{\lambda\mu 2}^{+}$, $\mathbf{v}_{\lambda\mu 0}^{-}$, $\mathbf{v}_{lm 2}^{1+}$, $\mathbf{v}_{lm 0}^{1-}$ to render the uniqueness of the basis solutions for chosen values of $A_{\lambda\mu}^{+}$ and A_{lm}^{1+} . In Appendix A, we prove (3.16) and justify how it can be used to determine the gauge dependent Stokesian basis functions.

If (3.16) is used to define the basis solutions, a major simplification can be achieved in the analysis. By expanding $\mathbf{v}_{lm\sigma}^{1-}(\mathbf{r})$ in terms of $\mathbf{v}_{\lambda\mu\sigma'}^{-}(\mathbf{r})$ as in (2.10) and $\mathbf{v}_{\lambda\mu\sigma'}^{+*}(\mathbf{r}')$ in terms of $\mathbf{v}_{lm\sigma}^{1+*}(\mathbf{r}')$ as in (2.11) for the same conduit-particle configuration (i.e. for same \mathbf{R}), and equating the two summation series of outer products in (3.16), we get

$$\sum_{\lambda\mu\sigma'} \sum_{lm\sigma} \mathbf{v}_{lm\sigma}^{1+*}(\mathbf{r}') T_r^*(\mathbf{R} | lm\sigma, \lambda\mu\sigma') \mathbf{v}_{\lambda\mu\sigma'}^{-}(\mathbf{r}) = \sum_{\lambda\mu\sigma'} \sum_{lm\sigma} \mathbf{v}_{lm\sigma}^{1+*}(\mathbf{r}') T_f(\lambda\mu\sigma', lm\sigma | \mathbf{R}) \mathbf{v}_{\lambda\mu\sigma'}^{-}(\mathbf{r}). \quad (3.17)$$

The above equation is true for all possible \mathbf{r} and \mathbf{r}' as long as $\rho_R < \rho$ (ρ_R being related to \mathbf{R}). Such general equality is possible only if

$$T_f(\lambda\mu\sigma', lm\sigma | \mathbf{R}) = T_r^*(\mathbf{R} | lm\sigma, \lambda\mu\sigma'). \quad (3.18)$$

Such a relation between two types of transformation coefficients is an alternative version of well known reciprocal theorem. The benefit of (3.18) is that if T_r is calculated T_f becomes known immediately.

3.3. Basis solutions and transformation coefficients

Finally, in this subsection, we integrate all the elements of the analysis that have been discussed so far, and present the explicit expressions for each term in our main equation (2.18). For numerical implementations, these final results are to be substituted in (2.18) which relates amplitudes $c_{lm\sigma}^{-}$ with known coefficients $d_{lm\sigma}$. The motion inducing quantities like force and torque on the sphere as well as pressure differential in the conduit are described by $c_{lm\sigma}^{-}$. On the other hand, motion inducing quantities like translational and rotational velocities of the sphere, as well as mean flow in the channel are defined by $d_{lm\sigma}$. Hence, our final explicit relation between

these two sets of amplitudes helps us to provide comprehensive results involving the general Stokesian dynamics of the sphere-cylinder system. In spite of the complexity of the mathematical analysis, one can reproduce such results by using the derived expressions summarized here and following the outlined numerical procedures in the subsequent section.

By combining (3.3), (3.4), (3.11)–(3.13), (3.16) and setting $A_{\lambda\mu}^+ = A_{\lambda\mu}^- = 2\pi$, $q^+ = q^{-*} = i$, we derive $v_{\lambda\mu\sigma}^\pm$ in the form described by (2.1). Accordingly, we first find

$$e_{\lambda\mu 0} = e^- \frac{e^{i(\mu\beta + \lambda z)}}{2\pi}, \quad e_{\lambda\mu 1} = e^+ \frac{e^{i(\mu\beta + \lambda z)}}{2\pi}, \quad e_{\lambda\mu 2} = e_z \frac{e^{i(\mu\beta + \lambda z)}}{2\pi}, \quad (3.19)$$

where

$$e^- = \frac{e_x - ie_y}{\sqrt{2}} e^{i\beta}, \quad e^+ = \frac{e_x + ie_y}{\sqrt{2}} e^{-i\beta}, \quad (3.20)$$

with e_z being the unit vector along the conduit axis, and e_x and e_y being mutually perpendicular unit vectors in a plane perpendicular to z . Then we complete the description of $v_{\lambda\mu\sigma}^\pm$ by expressing $f_{\lambda\mu s\sigma}^\pm$ as the $(\sigma + 1, s + 1)$ th element of 3×3 matrices $F_{\lambda\mu}^\pm$:

$$F_{\lambda\mu}^+ = \begin{bmatrix} \frac{\lambda I_{\mu+1}(\lambda\rho)}{\sqrt{2}} & \frac{i I_{\mu+1}(\lambda\rho)}{\sqrt{2}} & \frac{\rho(I_{\mu+2}(\lambda\rho) + I_\mu(\lambda\rho))}{4\sqrt{2}} \\ \frac{\lambda I_{\mu-1}(\lambda\rho)}{\sqrt{2}} & \frac{i I_{\mu-1}(\lambda\rho)}{\sqrt{2}} & \frac{\rho(I_\mu(\lambda\rho) + I_{\mu-2}(\lambda\rho))}{4\sqrt{2}} \\ i\lambda I_\mu(\lambda\rho) & 0 & i \frac{\lambda\rho I_{\mu+1}(\lambda\rho) + \lambda\rho I_{\mu-1}(\lambda\rho) + 2I_\mu(\lambda\rho)}{4\lambda} \end{bmatrix},$$

$$F_{\lambda\mu}^- = \begin{bmatrix} \frac{\rho(K_{\mu+2}(\lambda\rho) + K_\mu(\lambda\rho))}{4\sqrt{2}} & \frac{i K_{\mu+1}(\lambda\rho)}{\sqrt{2}} & \frac{\lambda K_{\mu+1}(\lambda\rho)}{\sqrt{2}} \\ \frac{\rho(K_\mu(\lambda\rho) + K_{\mu-2}(\lambda\rho))}{4\sqrt{2}} & \frac{i K_{\mu-1}(\lambda\rho)}{\sqrt{2}} & \frac{\lambda K_{\mu-1}(\lambda\rho)}{\sqrt{2}} \\ -\frac{\lambda\rho K_{\mu+1}(\lambda\rho) + \lambda\rho K_{\mu-1}(\lambda\rho) - 2K_\mu(\lambda\rho)}{4\lambda} & 0 & i\lambda K_\mu(\lambda\rho) \end{bmatrix}, \quad (3.21)$$

and proving \mathbf{S} to be the identity tensor \mathbf{I} . The conduit reflection is evaluated using $F_{\lambda\mu}^\pm$,

$$R_c(\lambda\mu; a) = [F_{\lambda\mu}^+(a)]^{-1} [F_{\lambda\mu}^-(a)], \quad (3.22)$$

where the $(\sigma_1 + 1, \sigma_2 + 1)$ th element of $R_c(\lambda\mu; a)$ represents reflection coefficients $R_c(\lambda\mu\sigma_1\sigma_2; a)$.

In a similar way, combining (3.5), (3.6), (3.11)–(3.13), (3.16) and setting $A_{lm}^{1+} = 1$, $A_{lm}^{1-} = 2l + 1$, $q^{1+} = q^{1-*} = i$, we obtain $v_{lm\sigma}^{1\pm}$ defined in (2.2). We find $\mathbf{S}_1 = \mathbf{I}$,

$$e_{lm0}^1 = e_r Y_{lm}, \quad e_{lm1}^1 = r e_r \times \nabla Y_{lm}, \quad e_{lm2}^1 = r \nabla Y_{lm}, \quad (3.23)$$

where $1 < l < \infty$, $-l \leq m \leq l$, and express $f_{lms\sigma}^{1\pm}$ in terms of the $\sigma + 1, s + 1$ th element of $\mathbf{F}_{lm}^{1\pm}$:

$$\mathbf{F}_{lm}^{1+} = \begin{bmatrix} lr^{l-1} & 0 & \frac{lr^{l+1}}{2(2l+3)} \\ 0 & \frac{ir^l}{l+1} & 0 \\ r^{l-1} & 0 & \frac{(l+3)r^{l+1}}{2(l+1)(2l+3)} \end{bmatrix}, \quad \mathbf{F}_{lm}^{1-} = \frac{1}{2l+1} \begin{bmatrix} \frac{(l+1)r^{-l}}{2(2l-1)} & 0 & -(l+1)r^{-l-2} \\ 0 & \frac{ir^{-l-1}}{l} & 0 \\ \frac{(l-2)r^{-l}}{2l(2l-1)} & 0 & r^{-l-2} \end{bmatrix}. \quad (3.24)$$

Then we construct

$$\mathbf{R}_p(lm; a_1) = [\mathbf{F}_{lm}^{1+}(a_1)]^{-1} [\mathbf{F}_{lm}^{1-}(a_1)], \quad (3.25)$$

to represent reflection coefficients $R_p(lm\sigma_1\sigma_2; a_1)$ as the $(\sigma_1 + 1, \sigma_2 + 1)$ th element of $\mathbf{R}_p(lm; a_1)$.

Once the basis solutions for cylindrical and spherical coordinates are derived, the transformation coefficients as defined in (2.10) and (2.11) are determined. For a single sphere inside a cylinder, the coordinates and origins are chosen in such a way that the relative position is given by $\mathbf{R} = R\mathbf{e}_x$. For such a configuration, we use Taylor series expansion to calculate

$$T_r(lm2, \lambda\mu2) = C_{lm}H(\lambda, \mu; l, m), \quad (3.26)$$

$$T_r(lm1, \lambda\mu2) = -\frac{im}{\lambda l} C_{lm}H(\lambda, \mu; l, m), \quad (3.27)$$

$$T_r(lm0, \lambda\mu2) = \frac{l(l-1)(2l-1) - (l^2 - m^2)(l-2)}{2\lambda^2 l(2l-1)} C_{lm}H(\lambda, \mu; l, m) \\ - \frac{R}{4\lambda^2} C_{lm}[H(\lambda, \mu; l+1, m-1) - H(\lambda, \mu; l+1, m+1)], \quad (3.28)$$

where

$$H(\lambda, \mu; l, m) = \frac{2}{\sqrt{\pi}} (i\lambda)^l (i^m) I_{|m-\mu|}(\lambda R), \quad C_{lm} = \frac{1}{\sqrt{4(l-m)!(l+m)!(2l+1)}}. \quad (3.29)$$

The derivation of these coefficients is presented in Appendix B. From the listed coefficients in (3.26)–(3.28), one can evaluate all coefficients in T_f and T_r with the help of (3.7)–(3.10), (3.18).

4. Numerical implementation

The main objective of our numerical simulation is to compute the hydrodynamic force and torque on the particle inside the cylinder. We relate the external force and torque on the particle to its linear and angular velocities by using generalized friction tensors. The contribution of a pressure-driven parabolic flow impinging from infinity is also included in the formulation. Considering net force and torque on the suspended inertialess body to be zero, one finds

$$\mathbf{F}^{ft} \cdot \mathbf{u} + \mathbf{F}^{fr} \cdot \boldsymbol{\omega} + \mathbf{f}^p + \mathbf{f}^{ex} = 0, \quad (4.1)$$

and

$$\mathbf{F}^{rt} \cdot \mathbf{u} + \mathbf{F}^{rr} \cdot \boldsymbol{\omega} + \boldsymbol{\tau}^p + \boldsymbol{\tau}^{ex} = 0. \quad (4.2)$$

In (4.1) and (4.2), \mathbf{u} and $\boldsymbol{\omega}$ are the translational and rotational velocities. The viscous force and torque on a fixed sphere in presence of a parabolic flow are given by \mathbf{f}^p

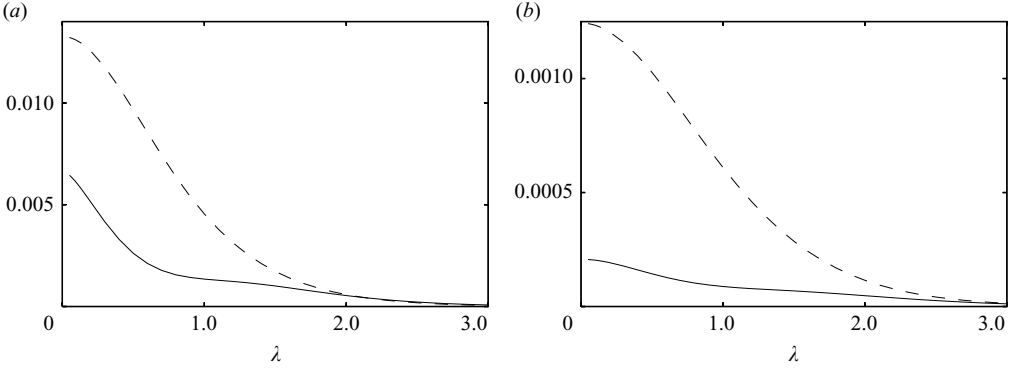


FIGURE 2. The integrand in (4.5) for $l = 1$, $m = 0$, $l'' = 1$, $m'' = 0$ as a function of λ with $\mu = 1(a)$ and $\mu = 2(b)$ when $a = 2a_1$ and $\mathbf{R} = 0.5a_1\mathbf{e}_x$. The solid and dashed lines correspond to $\sigma = \sigma'' = 0$ and $\sigma = \sigma'' = 1$.

and $\boldsymbol{\tau}^p$, and the external force and torque on the suspended body are \mathbf{f}^{ex} and $\boldsymbol{\tau}^{ex}$. The second-order tensors \mathbf{F}^{tt} , \mathbf{F}^{rr} , \mathbf{F}^{lr} and \mathbf{F}^{rl} are friction tensors with \mathbf{F}^{lr} being the transpose of \mathbf{F}^{rl} . In our analysis, we first evaluate \mathbf{F}^{tt} , \mathbf{F}^{rr} , \mathbf{F}^{lr} , \mathbf{F}^{rl} , \mathbf{f}^p and $\boldsymbol{\tau}^p$. Then from (4.1) and (4.2) we also calculate \mathbf{u} and $\boldsymbol{\omega}$ for a freely moving particle where $\mathbf{f}^{ex} = 0$ and $\boldsymbol{\tau}^{ex} = 0$.

We find the aforementioned quantities by solving the linear system of equations in (2.18) which relates $c_{l'm'\sigma'}$ to known $d_{lm\sigma}$. One can invert these equations and gets

$$c_{l'm'\sigma'} = \sum_{lm\sigma} L(l'm'\sigma', lm\sigma) d_{lm\sigma}. \quad (4.3)$$

The coupling constants $L(l'm'\sigma', lm\sigma)$ correspond to the inverse of the relation in (2.18)

$$\sum_{lm\sigma} L(l'm'\sigma', lm\sigma) M(lm\sigma, l''m''\sigma'') = \delta_{l'l''} \delta_{m'm''} \delta_{\sigma'\sigma''}, \quad (4.4)$$

where

$$M(lm\sigma, l''m''\sigma'') = R_p(lm\sigma\sigma''; a_1) \delta_{ll''} \delta_{mm''} - \sum_{\sigma_1\sigma_2} \sum_{\mu=-\infty}^{\infty} \int_{-\infty}^{\infty} T_r(lm\sigma, \lambda\mu\sigma_1) R_c(\lambda\mu\sigma_1\sigma_2; a) T_f(\lambda\mu\sigma_2, l''m''\sigma'') d\lambda. \quad (4.5)$$

The integrands in (4.5) for any given l , m , σ , l'' , m'' , σ'' are fast decaying functions of λ . A few of these integrands are plotted in figure 2 with varying λ . Also, the figure suggests a fast convergence of the integrand values with increase in μ . We can observe that the integrand is reduced by order of magnitudes when μ increases from 1 to 2.

Generally, \mathbf{L} and \mathbf{M} are referred as the grand friction and grand mobility matrices, respectively. The components of \mathbf{F}^{tt} , \mathbf{F}^{rr} , \mathbf{F}^{lr} , \mathbf{F}^{rl} , \mathbf{f}^p , $\boldsymbol{\tau}^p$ are related to various linear combinations of $\mathbf{L}(l'm'\sigma', lm\sigma)$. For example, the axial translational friction F_{zz}^{tt} is proportional to the element $\mathbf{L}(100, 100)$. Similarly, both radial ($F_{\rho\rho}^{tt}$) and azimuthal ($F_{\beta\beta}^{tt}$) frictions are determined from $\mathbf{L}(110, 110)$, $\mathbf{L}(1-10, 1-10)$, $\mathbf{L}(1-10, 110)$, $\mathbf{L}(110, 1-10)$.

So in our simulation, we first compute \mathbf{M} by numerically integrating over λ and summing over σ_1 , σ_2 and μ . Then we invert the matrix representing \mathbf{M} to calculate

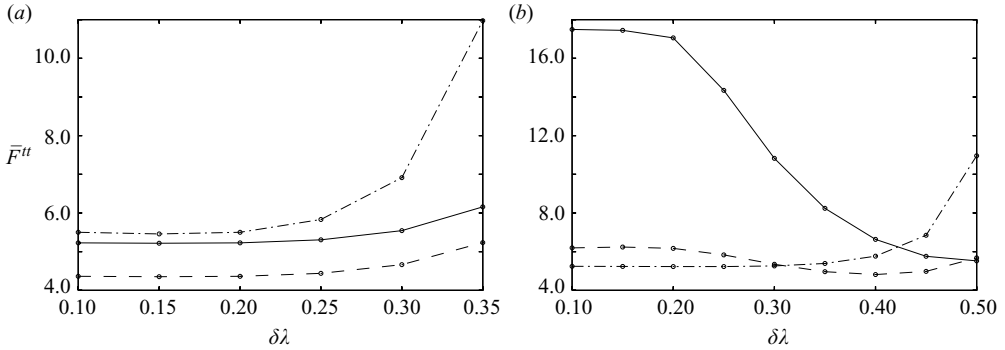


FIGURE 3. Computed values of diagonal elements of translational friction \mathbf{F}^{tt} as functions of interval $\delta\lambda$ for numerical integral when $a = 2a_1$. We plot radial component $F_{\rho\rho}^{tt}$ (solid lines), azimuthal component $F_{\beta\beta}^{tt}$ (dashed line) and axial component F_{zz}^{tt} (dash-dot line) for moderate separation between the surfaces of cylinder and sphere with $R = 0.5a_1$ (a) as well as for nearly touching configuration with $R = 0.9a_1$ (b).

L. Finally, the relevant quantities are extracted from different linear combinations of $\mathbf{L}(l'm'\sigma', lm\sigma)$. However, there can be numerical errors because of inherent approximations in the process. Firstly, the construction of M is inaccurate because of the involved numerical summations and integrations. Secondly, an error is introduced in the inversion of M because the infinite set of coefficients are truncated at some finite value. In the next two subsections, we present representative convergence tests to provide an estimate of these two types of error for a few critical elements.

4.1. Errors in construction of the grand mobility matrix

We identify three numerical approximations in the evaluation of M . First of all, the interval length for the numerical integration in λ is denoted by $\delta\lambda$ which is finite. Then the numerical integration is truncated at a certain Λ_{max} instead of ∞ so that the integration on λ is from $-\Lambda_{max}$ to Λ_{max} . Finally, the infinite summation over μ is truncated so that in simulation it is actually from $-\mu_{max}$ to μ_{max} . Hence, we choose the diagonal elements of \mathbf{F}^{tt} as representative cases and study convergences on $\delta\lambda$, Λ_{max} and μ_{max} . We select these particular elements because these are the most crucial friction elements and at the same time are more prone to convergence problems.

In figure 3, the computed translational frictions are presented as a function of $\delta\lambda$. In this study, two configurations are considered where the particle centre is either in the middle of the cylinder surface and cylinder centre or very near to the cylinder surface. In both cases, the cylinder radius a is twice of the sphere radius a_1 . We employed a cubic integral scheme where we assign $\Lambda_{max} = 12.0$. The other numerical parameter μ_{max} is assumed to be 12. The figure shows that the convergence of the curves to a particular value is very fast. When the particle is away from the wall with $R = 0.5a_1$ the convergence is relatively better. We check that the order of convergence for low $\delta\lambda$ is between 3 and 4.

Next, we focus on the convergence of the same quantities with respect to Λ_{max} for the same configurations. For these studies, we consider $\delta\lambda = 0.1$ and $\mu_{max} = 12$. These results are presented in figure 4 from which one can conclude that the values converge well at $\Lambda_{max} = 5.0$. Again, we find that the convergence is better for $R = 0.5a_1$.

In figure 5, we show how the values converge with μ_{max} where $\delta\lambda = 0.1$ and $\Lambda_{max} = 12$. It can be concluded that for $\mu_{max} = 5$, a reasonable convergence is achieved for all configurations.

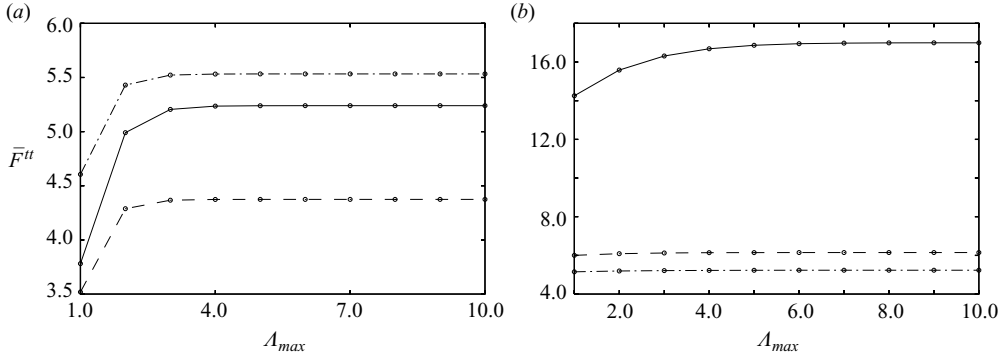


FIGURE 4. Same as figure 3 except computed quantities are presented as functions of integration limit Λ_{max} instead of $\delta\lambda$ for $R = 0.5a_1$ (a) and $R = 0.9a_1$ (b).

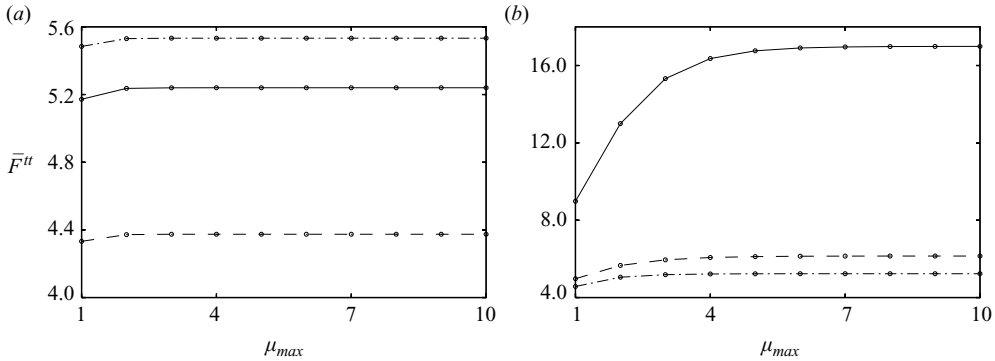


FIGURE 5. Same as figure 3 except computed quantities are presented as functions of summation limit μ_{max} instead of $\delta\lambda$ for $R = 0.5a_1$ (a) and $R = 0.9a_1$ (b).

We notice the common trend where the convergences are better for a particle situated at an intermediate point like at $R = 0.5a_1$ than for the particle very near to the cylindrical wall. The reason behind such convergence characteristics is the fact that when the particle is near the cylinder periphery we need more cylindrical basis solutions (i.e. more Λ_{max} and μ_{max}) to describe the scattered flow-field from the particle at the conduit surface. The number of required cylindrical basis is related to the angle sustained by the particle at the axis of the cylinder – more solutions are needed for a smaller angle. Hence further the particle is from the periphery, lower are the necessary values for Λ_{max} and μ_{max} .

For all cases the simulation time for one configuration is of the order of a few seconds. Moreover, due to the convergence properties, the scheme is even more efficient for intermediate particle positions than for peripheral positions. This enhanced efficiency for intermediate positions is an extra benefit for analysis of confined particulate systems because in such configurations asymptotic methods do not work.

4.2. Approximation in solution of the linear systems of equation

Ideally, in the matrix $M(l'm'\sigma', lm\sigma)$, the integer indices l' and l vary from 1 to ∞ . In practice, the infinite dimensional matrix M is truncated to a certain dimension and then inverted to evaluate M approximately. Accordingly, we assign a maximum value l_{max} for both l and l' , and construct the matrix \mathbf{L} representing $\mathbf{L}(l'm'\sigma', lm\sigma)$ with the primed and unprimed indices corresponding to rows and columns, respectively.

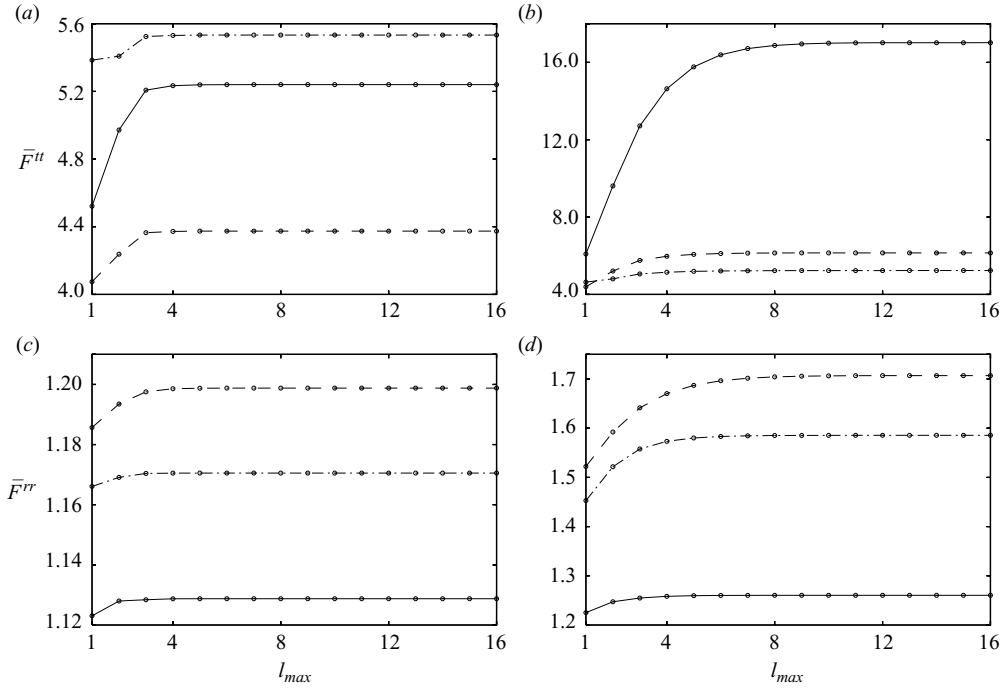


FIGURE 6. Computed values of diagonal elements of translational friction \mathbf{F}^{tt} and rotational friction \mathbf{F}^{rr} as functions of l_{max} representing the number of basis functions considered in the simulation. The configurations and line types for radial, azimuthal and axial components are same as figure 3.

Consequently for $-l' \leq m' \leq l'$, $-l \leq m \leq l$ and $\sigma, \sigma' = 0, 1, 2$, one can determine the dimension of the matrix to be $q \times q$ where $q = 3l_{max}(l_{max} + 2)$.

The error in \mathbf{L} due to truncation in the dimension of \mathbf{M} is manifested by a convergence test (known as spectral convergence) which demonstrates how the friction coefficients saturate to a certain value with increasing l_{max} . We present these results in figure 6 where we plot diagonal elements of \mathbf{F}^{tt} and \mathbf{F}^{rr} as functions of l_{max} . We consider $a = 2a_1$ and two cases with $R = 0.5a_1$ and $R = 0.9a_1$.

The results show that all quantities converge well at $l_{max} = 6$ which is a very small number. This is even true for usually critical cases where particle is very near to the conduit surface. For a similar gap between surfaces of the particle and the confinement, planar wall geometry requires $l_{max} = 16$ for reasonable convergence (Bhattacharya *et al.* 2005a,b). The reason behind this difference is simple. For a sphere near a planar wall, the angular variation in geometry is more than a sphere inside a cylinder. To resolve larger azimuthal variation around the sphere, a larger l_{max} is necessary for convergence. As a result, cylindrical geometries exhibit relatively better spectral convergence than planar-wall geometries. This is a major advantage for our simulation which requires less than a minute to provide a reasonable result with relative error less than 1% for a particular configuration.

5. Hydrodynamic resistance in quiescent fluid inside a cylinder

We apply the simulation algorithm to comprehensively describe force and torque on a sphere due to its motion in a quiescent fluid in terms of friction coefficients

defined in (4.1) and (4.2). Because of the symmetries involved in the problem, one can prove that both \mathbf{F}^{tt} and \mathbf{F}^{rr} are diagonal matrices:

$$\mathbf{F}^{tt} = F_{\rho\rho}^{tt} \mathbf{e}_\rho \mathbf{e}_\rho + F_{\beta\beta}^{tt} \mathbf{e}_\beta \mathbf{e}_\beta + F_{zz}^{tt} \mathbf{e}_z \mathbf{e}_z, \quad \mathbf{F}^{rr} = F_{\rho\rho}^{rr} \mathbf{e}_\rho \mathbf{e}_\rho + F_{\beta\beta}^{rr} \mathbf{e}_\beta \mathbf{e}_\beta + F_{zz}^{rr} \mathbf{e}_z \mathbf{e}_z, \quad (5.1)$$

where \mathbf{e}_ρ , \mathbf{e}_β , \mathbf{e}_z are unit vectors along radial, azimuthal and axial directions. In contrast, the translation-rotation coupling tensors \mathbf{F}^{tr} and \mathbf{F}^{rt} , have the following forms:

$$\mathbf{F}^{tr} = -G \mathbf{e}_\beta \mathbf{e}_z - G' \mathbf{e}_z \mathbf{e}_\beta, \quad \mathbf{F}^{rt} = -G' \mathbf{e}_\beta \mathbf{e}_z - G \mathbf{e}_z \mathbf{e}_\beta, \quad (5.2)$$

which show that \mathbf{F}^{tr} and \mathbf{F}^{rt} are transpose of each other. Hence, it is possible to analyse the dynamics of the particle in a stagnant fluid inside a cylinder, if one determines eight friction coefficients: $F_{\rho\rho}^{tt}$, $F_{\beta\beta}^{tt}$, F_{zz}^{tt} , $F_{\rho\rho}^{rr}$, $F_{\beta\beta}^{rr}$, F_{zz}^{rr} , G , G' . We evaluate these scalar quantities for various configurations defined by non-dimensional length parameters $R/(a - a_1)$ and a/a_1 . We especially select those cases which are particularly difficult to be investigated by available asymptotic methods. For tighter configurations, a supplementary document present the values for all friction coefficients in tabular form.

5.1. Force on a translating sphere

In figure 7, non-dimensional components of \mathbf{F}^{tt} are presented where the quantities are normalized by the Stokesian friction of the sphere in free-space,

$$\bar{F}_{ii}^{tt} = \frac{F_{ii}^{tt}}{6\pi a_1 \eta}, \quad (5.3)$$

with i being either ρ or β or z . We plot $\bar{F}_{\rho\rho}^{tt}$, $\bar{F}_{\beta\beta}^{tt}$, \bar{F}_{zz}^{tt} as functions of normalized distance $R/(a - a_1)$ of the centre of the sphere from the axis of the cylinder so that the non-dimensional distance is always between 0 and 1. In the figures, the ratio a/a_1 varies as a parameter for different curves.

If the sphere is enclosed more closely by the cylindrical surface, the friction coefficients increase because of enhanced viscous interactions. This behaviour is evident in figure 7 which shows higher values of friction for smaller a/a_1 .

Generally, when the particle is nearer to the conduit wall, hydrodynamic resistance is more due to lubrication effects. This is why as R increases, the friction coefficients usually increase in a monotonous way. This general trend can be seen for $\bar{F}_{\rho\rho}^{tt}$ and $\bar{F}_{\beta\beta}^{tt}$ consistently or for \bar{F}_{zz}^{tt} when $a/a_1 \gg 1$. The exception to this behaviour happens when the particle is moving in axial direction, and the cylinder has small cross-section. In such cases where the sphere is substantially blocking the channel, two phenomena influence the motion of the particle. Firstly, during the axial motion, the particle acts like a piston, and a pressure difference is generated across it in axial direction. This difference in the pressure field hinders the particle. Secondly, if the sphere is very near to the conduit surface, lubrication stresses due to relative motion between the particle and the confinement also contribute in the hydrodynamic resistance. When the particle is centrally placed the pressure difference is maximum. Any shift from this position causes a release in pressure through the widened portion of the particle-wall gap, and its effect diminishes. On the other hand, lubrication stresses are maximum at the peripheral position. Hence, if $a \sim a_1$ we see a non-monotonous behaviour where for increasing R , first \bar{F}_{zz}^{tt} decreases due to reduced pressure difference and then increases due to enhanced lubrication stresses.

For a centrally situated sphere inside the cylinder, rotational symmetry dictates $\bar{F}_{\rho\rho}^{tt} = \bar{F}_{\beta\beta}^{tt}$. Actually, for such axisymmetric configuration, all translational friction

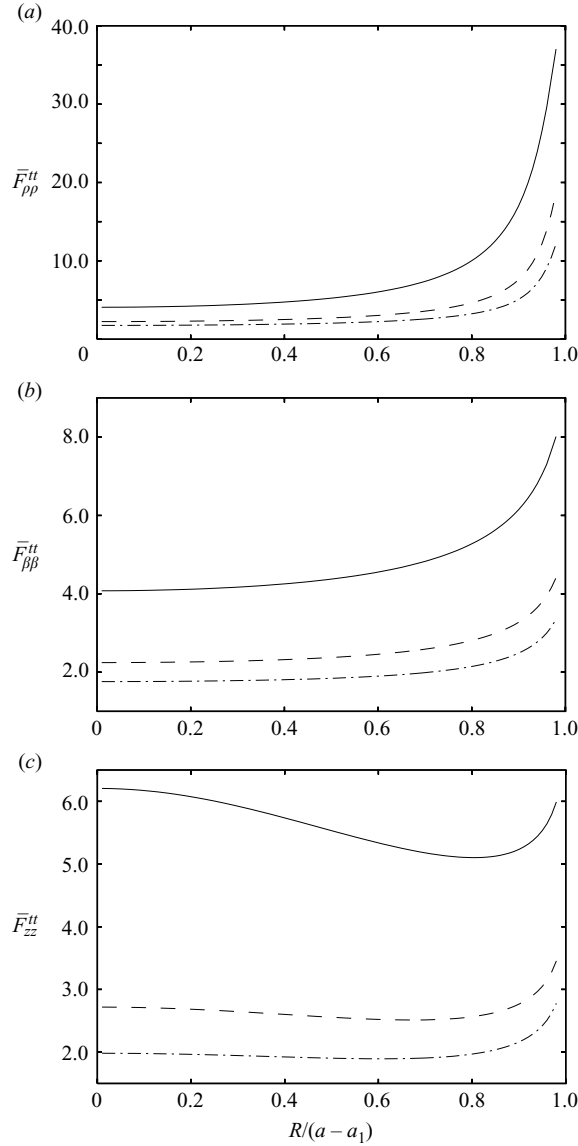


FIGURE 7. Normalized diagonal elements of the translational friction \mathbf{F}^{tt} versus radial position of the sphere-centre for $a = 2a_1$ (solid line), $a = 3a_1$ (dashed line), $a = 4a_1$ (dash-dot line).

components $\bar{F}_{\rho\rho}^{tt}$, $\bar{F}_{\beta\beta}^{tt}$, \bar{F}_{zz}^{tt} have more or less similar values. However, when the particle is placed in an off-centred position the radial component $\bar{F}_{\rho\rho}^{tt}$ varies differently than $\bar{F}_{\beta\beta}^{tt}$ and \bar{F}_{zz}^{tt} . For radial motion, the sphere moves normally towards the bounding surface and encounters a resistance which is inversely proportional to the gap between the approaching surfaces. The explanation is well known – lubrication fields cause a sharp increase in $\bar{F}_{\rho\rho}^{tt}$ for an increase in R when the particle is at the periphery of the cylinder. Similar trend is evident for axial and azimuthal frictions also, but the increase is relatively slower for $\bar{F}_{\beta\beta}^{tt}$ and \bar{F}_{zz}^{tt} than for $\bar{F}_{\rho\rho}^{tt}$. For $\bar{F}_{\beta\beta}^{tt}$ and \bar{F}_{zz}^{tt} , the motion of the sphere is mainly tangential to the confining wall. Such motion creates a weaker lubrication field that is responsible for the hydrodynamic friction

varying logarithmically with inter-surface gap. The logarithmic variation is weaker than inversely proportional increase. As a result, $\bar{F}_{\beta\beta}^{tt}$ and \bar{F}_{zz}^{tt} are smaller than $\bar{F}_{\rho\rho}^{tt}$ when the particle is at the periphery of the cylinder.

Between $\bar{F}_{\beta\beta}^{tt}$ and \bar{F}_{zz}^{tt} , the latter is larger at the central position due to the developed pressure difference in piston-like axial motion. The situation reverses in the peripheral position because of lubrication fields. Lubrication effect is more prominent for azimuthal motion compared to axial motion. This happens because azimuthal motion is normally directed to some portion of the confinement and develops relatively stronger resistance. In contrast, the axial motion is entirely directed in a tangential direction to the vessel wall and causes weaker hydrodynamic friction.

5.2. Torque on a rotating sphere

The components of the rotational friction tensor \mathbf{F}^{rr} is normalized by the value corresponding to a sphere in unbounded fluid

$$\bar{F}_{ii}^{rr} = \frac{F_{ii}^{rr}}{8\pi a_1^3 \eta}, \quad (5.4)$$

where i is either ρ or β or z . In figure 8, the non-dimensional quantities $\bar{F}_{\rho\rho}^{rr}$, $\bar{F}_{\beta\beta}^{rr}$, \bar{F}_{zz}^{rr} are presented as functions of $R/(a - a_1)$ for different a/a_1 .

All the normalized components of \mathbf{F}^{rr} monotonously increase with increasing $R/(a - a_1)$ and decreasing a/a_1 because such changes in $R/(a - a_1)$ and a/a_1 enhance viscous interactions due to closer proximity of the particle to the conduit surfaces. For smaller gap between these two bodies, lubrication effect influences the hydrodynamic behaviour. As rotation produces a predominantly tangential relative motion between the touching surfaces, the resistance to the motion due to lubrication contribution varies logarithmically with the inter-surface gap. Thus, we observe a slower increase in $\bar{F}_{\rho\rho}^{rr}$, $\bar{F}_{\beta\beta}^{rr}$, \bar{F}_{zz}^{rr} with increasing $R/(a - a_1)$ compared to the behaviour of $\bar{F}_{\rho\rho}^{tt}$ which varies inversely proportional to the gap.

The figures illustrate the relative strength of $\bar{F}_{\rho\rho}^{rr}$, $\bar{F}_{\beta\beta}^{rr}$, \bar{F}_{zz}^{rr} which agrees with intuitive arguments. For the centrally placed particle, $\bar{F}_{\rho\rho}^{rr} = \bar{F}_{\beta\beta}^{rr}$ which is evident from figure 8. However, as the particle approaches the periphery of the cylinder $\bar{F}_{\beta\beta}^{rr}$ increases more than $\bar{F}_{\rho\rho}^{rr}$. The explanation is as follows: the velocity gradient due to relative velocity between the sphere and the cylinder surface for azimuthal rotation than that for the radial rotation. Consequently, the azimuthal rotation induces relatively more viscous interactions and more resistance compared to rotation in the radial direction. On the other hand, the gradients in velocity field due to relative velocity between the particle and conduit surfaces are comparable for both axial and azimuthal rotations. Accordingly, we find that $\bar{F}_{\beta\beta}^{rr}$ and \bar{F}_{zz}^{rr} have similar values for all $R/(a - a_1)$ and a/a_1 .

5.3. Translation-rotation coupling

When the sphere is not in the axisymmetric position, its rotation in a certain direction induces hydrodynamic force whereas its translation may generate torque on the suspended body. Symmetry dictates that only for radial translation and rotation such couplings are not possible. More specifically, if the particle rotates in the axial or azimuthal directions with its centre not on the conduit axis, it encounters a force in the azimuthal or axial directions, respectively. Similarly, if the particle translates in the axial or azimuthal directions, it experiences torque in the azimuthal or axial directions, respectively. These couplings between translational and rotational quantities are caused by the presence of the confinement and are quantified by the coefficients G and G' defined in (5.2).

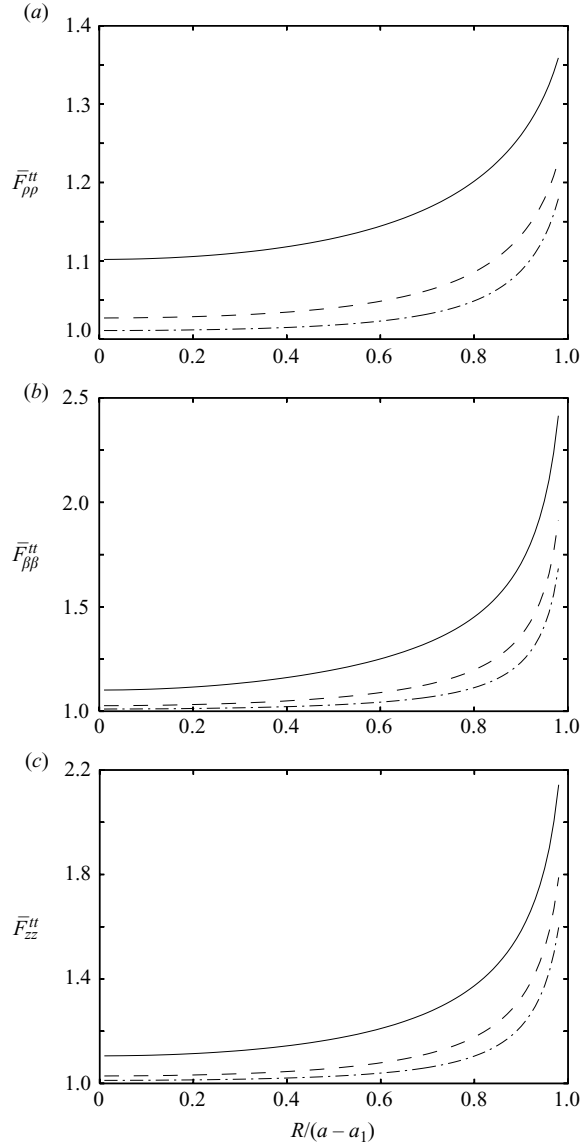


FIGURE 8. Same as figure 7 except normalized diagonal elements of the rotational friction \mathbf{F}^{rr} .

We non-dimensionalize G and G' with $a_1^2\eta$

$$\bar{G} = \frac{G}{a_1^2\eta} \quad \bar{G}' = \frac{G'}{a_1^2\eta}, \quad (5.5)$$

and plot \bar{G} and \bar{G}' for different $R/(a - a_1)$ and a/a_1 in figure 9. As expected, with $R = 0$ for the central position, $\bar{G} = \bar{G}' = 0$ due to axisymmetric configuration. For non-zero R , magnitudes of both coefficients generally increase with decrease in a/a_1 because such variation in relative dimension creates enhanced viscous interactions due to closer proximity between the particle and conduit. However, the behaviour of \bar{G} and \bar{G}' with respect to $R/(a - a_1)$ is not monotonous – we can see a reversal in

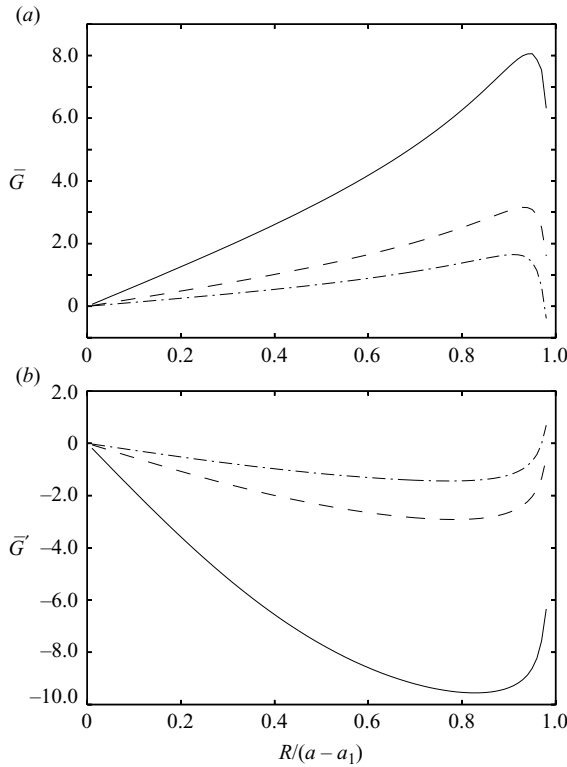


FIGURE 9. Normalized non-zero components of \mathbf{F}^r or \mathbf{F}^t as functions of non-dimensional position of the centre of the sphere. Interpretation of the line types are same as in figure 7.

trend and values for both cases. In the subsequent discussion, we intuitively explain this non-monotonic characteristic for both \bar{G} and \bar{G}' .

According to (5.2), G is the coefficient which relates either axial rotation with azimuthal force or azimuthal translation with axial torque. The behaviour of this coupling constant with increasing $R/(a - a_1)$ can be equivalently explained by considering either of these relations. When the particle rotates in the axial direction, two phenomena influence the hydrodynamic interactions. Firstly, in order to maintain a consistent volumetric flow in the gap between the surfaces of the sphere and the cylinder, the pressure field contains an angular variation that creates a net force in the azimuthal direction. Secondly, for a peripheral position of the particle inside the conduit, lubrication stresses due to the relative motion between the adjacent surfaces contribute in azimuthal force. These two effects are mutually opposing. Similar azimuthal pressure variation and lubrication effect can be observed for translating particles in the azimuthal direction where again both of these factors tend to cancel each other. The relative influence of the first contribution is stronger than that of the second when the sphere is near the cylinder centre and far away from the periphery. The relative effect of lubrication fields, however, increases when the particle approaches the wall. As a result, the trend in the variation of G with increasing R first reverses and the value starts to decay with R after reaching an extremum value. Then the value itself may change sign because of very strong lubrication. This reversal in trend is more prominent for moderate a/a_1 because in that case the pressure variation and the lubrication effect have equal contribution to create a noticeable difference.

The other coefficient G' exhibits a similar pattern of variation with increasing R . It couples either axial translation with azimuthal torque or azimuthal rotation with axial force. As in the case of G , here also spatial variation in pressure field plays a key role along with the near-contact lubrication effect. Only difference is that the variation in pressure field is along the axial direction instead of the angular direction. Again like before, these two effects are subtractive to each other, and near the axisymmetric configuration ($R \rightarrow 0$) the relative strength of the pressure differential is predominant over the lubrication effect. The situation reverses for peripheral position ($R \rightarrow a - a_1$). As a result, a change in trend after reaching an extremum value and ultimately a reversal in the sign of G' can be observed with increasing R .

5.4. Validation by comparing with the analytical results for limiting cases

We compare a few representative results from our simulation with the values obtained by using various perturbation analyses for different limiting cases. We already know that our computation agrees well with physically intuitive arguments. We also know that the convergence tests with respect to various computational parameters show a high convergence rate for the algorithm. Moreover, there are a couple of other consistency checks from theoretical point of view. Firstly, the integrand in (2.18) has singular components which are non-integrable over the wavenumber λ , and cancel each other to give an integrable function only if the analytical derivations are correct. Hence, any error in the derivation is ruthlessly exposed by the non-converging integral. Secondly, the matrix \mathbf{L} in (4.3) should be a positive definite matrix if calculated properly. We confirm that our formulation satisfies both these consistency conditions. All these tests are, however, necessary checks – they are not sufficient to prove absolute accuracy of our solution. For this purpose, we need some quantitative verification of the numerical study by comparing it with some known exact results.

For quantitative validation, we consider the available theoretical results for axial motion of the sphere in limiting configurations. First, we calculate the translational friction in the axial direction according to the lubrication theory for a closely fitted sphere in the cylinder (Bungay & Brenner 1973*b*). We assume the particle to be in axisymmetric position and compare our simulation with the theoretical values when $a \sim a_1$. Then, we use the reflection method in axisymmetric configuration and test how our computation matches with it for $a \gg a_1$. The comparison is presented in figure 10 where one can see that our results match perfectly with both theoretical curves in respective regimes. The computation agrees very well with (Bungay & Brenner 1973*b*) when $a \sim a_1$, but then starts to diverge as a increases. The trend is reverse with the reflection method which differs by less than 1% with the simulated values for $a > 5a_1$ and deviates when $a \sim a_1$.

In figure 11, we account for an eccentric position of the sphere with respect to the cylinder where $R = 2a_1$. For such R , one cannot expect the lubrication theory to give correct results for tightly fitted sphere. Hence, for eccentric configuration, we compare our result only with reflection method. Unlike the axisymmetric case, here we can compute non-zero G' along with F''_{zz} . We present both coefficients for a comparative study and find reasonable accuracy (within 1%) between our approach and reflection method when $a > 5R$. Two solutions diverge for lower values of a . For G' , this difference is more dramatic where the reversal in the magnitude is evident in the simulated data as $a \rightarrow (R + a_1)$. This reversal is due to the lubrication effect which reflection method cannot capture.

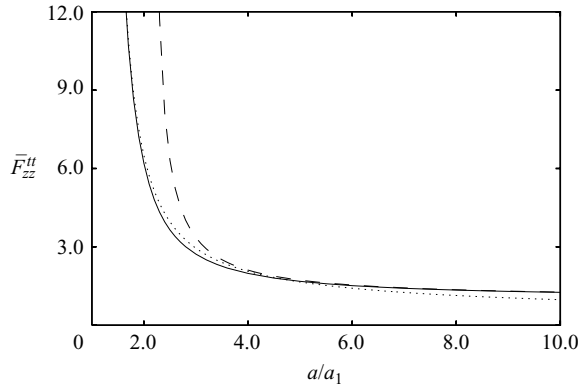


FIGURE 10. Computed values of axial friction for translation (solid line) in axisymmetric configuration are compared with reflection method (dashed line) for $a \gg a_1$ and singular perturbation method (dotted line) for $a \sim a_1$.

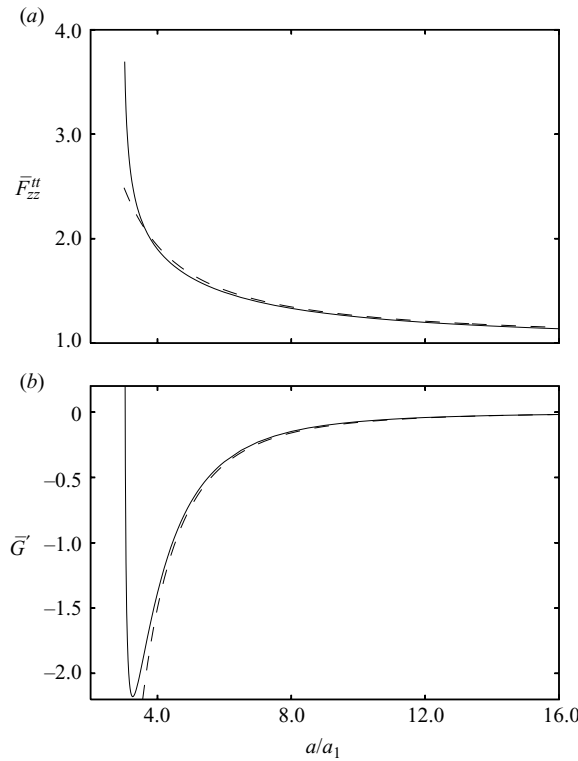


FIGURE 11. Computed values of friction coefficients (solid line) for off-centred position $R = 2a_1$ are compared with reflection method (dashed line) for $a \gg a_1, R$.

In table 1, we verify our results with the same obtained by using lubrication theory for tight configuration. We compute both F_{zz}^{tt} and G' for different R . The difference in two sets of values is within the error margin for lubrication theory.

Though we check the simulated values of only the axial frictions with existing results, this quantitative comparison is sufficient to give us confidence in the

	\bar{F}_{zz}''	\bar{F}_{zz}''	\bar{G}'	\bar{G}'
$R/(a - a_1)$	Lubrication	Simulation	Lubrication	Simulation
0.0	612	617	0	0
0.2	592	598	-128	-128
0.4	541	545	-239	-236
0.6	463	467	-303	-304
0.8	401	401	-350	-345
0.99	338	338	-354	-346

TABLE 1. A comparison between our simulation and the lubrication theory for a tight configuration with $a/a_1 = 1.1$. We use both approaches to obtain the normalized axial friction \bar{F}_{zz}'' and coupling coefficient \bar{G}' for different radial position of the particle. The lubrication results are good approximations with relative error $\sim 1\%$ for \bar{F}_{zz}'' and $\sim 3\%$ for \bar{G}' . The difference in two sets of results corresponds to the error limits indicating the validity of the formulation.

correctness of the entire analysis. In our method, the computation of the friction coefficients is interrelated because these are dependent on elements of the grand friction matrix \mathbf{L} which is constructed by inverting the computed grand mobility \mathbf{M} . Hence, correct evaluation of one set of coefficients implies the correctness of the other components of the friction tensors.

6. Particle motion in parabolic pressure-driven flow

Our final analysis involves the study of particle dynamics in a pressure-driven axial flow for which the variation in velocity profile is parabolic along the radial direction so that the velocity is maximum at the axis of symmetry and zero at the conduit surface. We address two problems here. Firstly, we consider a fixed sphere encountering the impending flow and calculate the force and torque on it. Then we determine the motion of the particle assuming that it is free to move under zero force and zero torque.

6.1. Force and torque on a fixed particle in parabolic velocity field

From symmetry arguments, one concludes that the force \mathbf{f}^p and the torque $\boldsymbol{\tau}^p$ in (4.1) and (4.2) can only have components in the z and β directions, respectively:

$$\mathbf{f}^p = f_z^p \mathbf{e}_z, \quad \boldsymbol{\tau}^p = \tau_\beta^p \mathbf{e}_\beta. \quad (6.1)$$

We normalize f_z^p and τ_β^p

$$\bar{f}_z^p = \frac{f_z^p}{6\pi a_1 \eta u_p}, \quad \bar{\tau}_\beta^p = \frac{\tau_\beta^p}{8\pi a_1^2 \eta u_p}, \quad (6.2)$$

where u_p is the velocity at the cylinder axis due to the parabolic flow. In figure 12, we plot the non-dimensional quantities \bar{f}_z^p and $\bar{\tau}_\beta^p$ as functions of $R/(a - a_1)$ for different a/a_1 .

The results show that \bar{f}_z^p and $\bar{\tau}_\beta^p$ consistently decrease with increasing a/a_1 because a smaller value of a ensures enhanced viscous interactions due to closer proximity between the particle and the conduit. For $R = 0$ at the axisymmetric configuration, $\bar{\tau}_\beta^p$ is always zero for any dimension of the cylinder or the sphere. Also, for axisymmetric position of the particle, $\bar{f}_z^p \rightarrow 1$ when $a/a_1 \rightarrow \infty$. Both these characteristics are noticeable in figure 12.

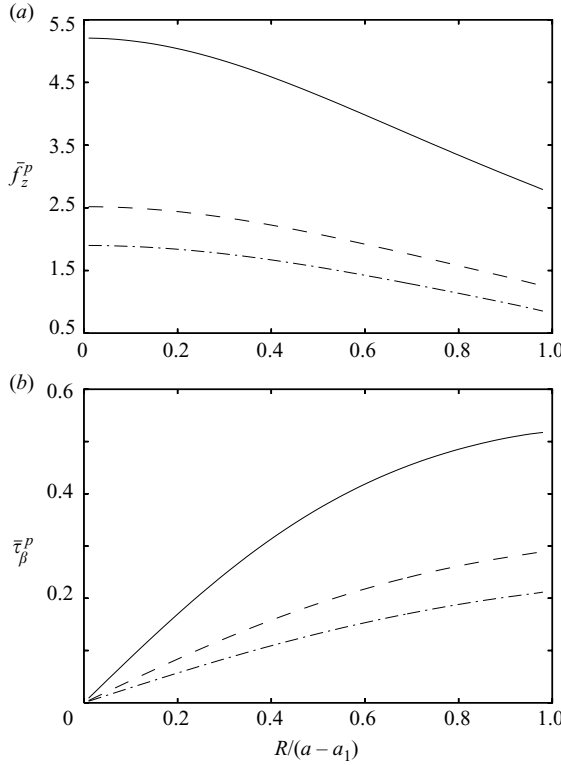


FIGURE 12. Normalized force and torque on a fixed sphere in parabolic flow as functions of its normalized radial position. The interpretation of the line types are same as in figure 7.

As $R/(a - a_1)$ increases, \bar{f}_z^p decreases for any a/a_1 . The magnitude of the force on the fixed particle is dependent on the magnitude of the local velocity due to the impending parabolic flow. The impending flow decreases with R due to the parabolic nature. As a result, the force is maximum in the axisymmetric position and decays as the particle approaches the cylinder periphery.

The trend of $\bar{\tau}_\beta^p$ with increasing $R/(a - a_1)$ is reverse. The torque is approximately proportional to the local shear rate which is zero at $R = 0$ and increases with R . As a result, when the particle moves away from the axis of the cylinder, $\bar{\tau}_\beta^p$ increases.

6.2. Motion of a free particle in Poiseuille flow

A free particle is free of inertia and external force so that the net viscous force and torque on it are zero. Hence, the motion of such particle can be determined by fixing $\mathbf{f}^{ex} = \mathbf{f} = \mathbf{0}$ and $\boldsymbol{\tau} = \boldsymbol{\tau}^{ex} = \mathbf{0}$. Accordingly, we solve (4.1) and (4.2) simultaneously to find \mathbf{u} and $\boldsymbol{\omega}$. Symmetry dictates

$$\mathbf{u} = u_z \mathbf{e}_z, \quad \boldsymbol{\omega} = \omega_\beta \mathbf{e}_\beta. \tag{6.3}$$

In figure 13, we present normalized u_z and ω_β as functions of $R/(a - a_1)$ for different a/a_1 .

For large values of a/a_1 , a free particle follows the fluid with a speed same as the local velocity of the impending field. As a result, it can be treated as a tracer particle, and the u_z versus R curve represents the parabolic velocity profile across the channel. We can observe this in figure 13. When the sphere is near the surface of the cylinder,

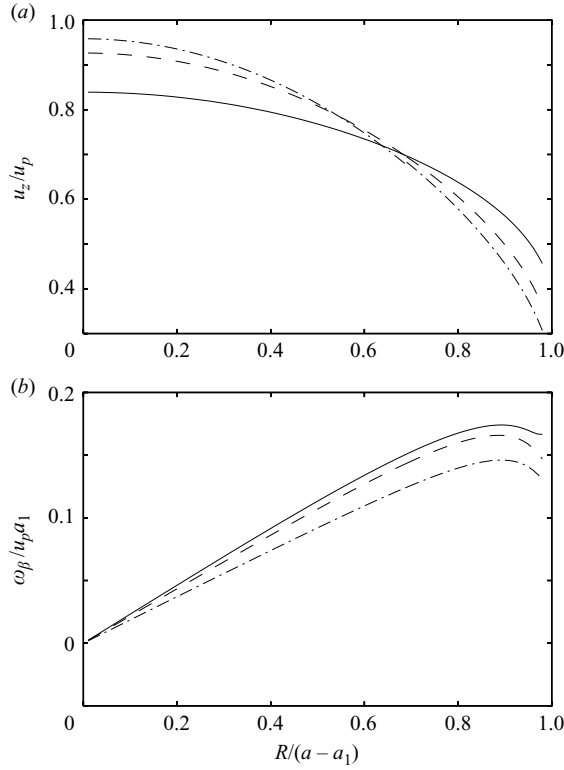


FIGURE 13. The linear and angular velocities of a free particle in pressure-driven parabolic flow as functions of its normalized radial position. The interpretation of the line types are same as in figure 7.

the curves depart from the parabolic function due to the effect of the reflected flow from the confinement. This departure is especially pronounced for narrow cylinders.

The rotational velocity of the sphere is proportional to the local shear of the impending flow. Accordingly, $\omega_\beta = 0$ at $R = 0$ as the shear is zero on the axis of the cylinder. The angular velocity increases linearly with R following the behaviour of the local shear for different radial positions. This characteristics is consistently manifested in figure 13. Exception happens only when the particle is very close to the wall. Then the angular velocity starts to decay with R because of the lubrication effect.

7. Summary and concluding remarks

In this paper, we outline a general mathematical procedure (basis transformation method) that can be used to develop fast algorithms to address fluid-mechanical problems involving suspended particles inside conduits. The method enables us to construct general reflection relations for the satisfaction of vector boundary conditions at disconnected simple surfaces. We specifically concentrate on solving Stokesian dynamics of a sphere in a cylinder. Unlike past analytical studies, the present method is applicable to all possible particle-conduit configurations, i.e. any dimension and particle position can be considered to define the system. The generality of our approach also allows us to describe not only the axial motion of the particle but also

all possible translations and rotations including those in the radial and azimuthal directions. To our knowledge, our results represent first such comprehensive study of the general motion of a spherical particle inside a cylindrical vessel.

The numerical scheme is extremely efficient because of the high convergence rates. According to our experience, we obtain reasonable results within 1 % accuracy using less than a minute of computational time in a 2 GHz machine. The relative errors in the simulation are found to be less than 1 % when the numerical results are compared with analytical values obtained from both lubrication theory and reflection method.

We present a few representative results for different relative dimensions of the sphere and the cylinder as well as for different radial positions of the particle. We especially choose the configurations where all three defining dimensions are comparable to each other because available asymptotic methods are not applicable in those cases. We consider the particle to be either undergoing a specified motion in quiescent fluid or encountering an impending pressure-driven parabolic flow. By definition, the first problem is a friction problem where hydrodynamic force and torque on the sphere are evaluated for a prescribed motion in stagnant fluid. For the second situation, however, one can furnish both friction and mobility descriptions. Accordingly, we evaluate the force and torque on a fixed particle in a parabolic flow (friction formulation) as well as determine the motion of a force-free torque-free particle in the same impending field (mobility formulation). The simulation results coincide properly with intuitive physical arguments.

We validate our simulation data in several ways. First of all, the convergence tests can be treated as necessary verification which, though cannot quantify absolute accuracy, can at least check consistency. Then there are two independent validations from the theoretical point of view. Integrability of the integrand in (2.18) is only ensured if the analytical derivations are correct. Secondly, the matrix \mathbf{L} in (4.3) should be positive definite which we confirm. Apart from these tests, we also compare our results with different asymptotic methods for limiting cases. The agreements between the two sets of results are satisfactory.

Though the primary focus of this article is on solving Stokesian fields around a sphere inside a cylinder where the velocity is specified at the solid–fluid interfaces, the outlined basis transformation method has a far more general applicability. As this method does not require symmetry constraints like recently proposed Cartesian representation method (Bhattacharya *et al.* 2005*a,b*), the presented formulation can be used in various situations. Hence, it can be applied to solve different second-order vector differential equations with linear boundary conditions specified at different disconnected simple surfaces. The only restriction on the governing equation and the geometries is that the basis solutions of the linear differential equation for the involved coordinate systems have to be in separable form as given by (2.1) and (2.2). Fortunately, for a wide range of fluid-mechanical problems, the separable basis solutions can be constructed.

In the future, we intend to explore all these possibilities. Most immediate generalization will be to extend this method to many-sphere system in a cylindrical conduit. There we need to modify the analysis by considering a number of spherical coordinates with origin at the centre of each particle and using the well-known transformation relations between spherical Stokesian solutions (Felderhof & Jones 1989). Furthermore, simple changes in the reflection relations would allow us to consider many body interactions in annular geometries. Finally, we can also apply basis transformation method to vector equations other than steady Stokes equation and to boundary conditions other than Dirichlet conditions. As a result, the problems

involving periodically oscillating fields (unsteady Stokes equation) or stress-free interfaces (Neumann condition) or surfactant covered surfaces (mixed boundary conditions) can also be addressed.

This work has been supported by ACS Petroleum Research Foundation grant PRF#49053-DN19.

Appendix A. Expansion of Oseen tensor

In this appendix, we prove (3.16) and show how this equation can be used as an additional constraint to determine unique expressions for gauge-field dependent Stokesian basis functions by fixing the gauge fields. In the derivation, the focus will be only on the first part of (3.16) describing the expansion of Oseen tensor in cylindrical basis as the second part involving the spherical basis can be implied by considering similar steps.

A.1. General expansion of a tensorial solution of Stokes equation

As $\mathbf{b} \cdot \mathbf{T}(\mathbf{r} - \mathbf{r}')$ is a solution of Stokes equation in both \mathbf{r} and \mathbf{r}' space for any constant vector \mathbf{b} , one can expand \mathbf{T} in terms of Stokesian basis functions:

$$\mathbf{T}(\mathbf{r} - \mathbf{r}') = \sum_{\lambda\mu\sigma} \sum_{\lambda'\mu'\sigma'} C_{\lambda\mu\lambda'\mu'}^{\sigma\sigma'} \mathbf{v}_{\lambda\mu\sigma}^+(\mathbf{r}) \mathbf{v}_{\lambda'\mu'\sigma'}^-(\mathbf{r}') \quad \text{when } \alpha < \alpha', \quad (\text{A } 1)$$

and

$$\mathbf{T}(\mathbf{r} - \mathbf{r}') = \sum_{\lambda\mu\sigma} \sum_{\lambda'\mu'\sigma'} C_{\lambda\mu\lambda'\mu'}^{\sigma\sigma'} \mathbf{v}_{\lambda\mu\sigma}^-(\mathbf{r}) \mathbf{v}_{\lambda'\mu'\sigma'}^+(\mathbf{r}') \quad \text{when } \alpha > \alpha'. \quad (\text{A } 2)$$

At $\alpha = \alpha'$, both expressions of \mathbf{T} should be the same implying $C_{\lambda\mu\lambda'\mu'}^{\sigma\sigma'} = C_{\lambda'\mu'\lambda\mu}^{\sigma'\sigma}$.

Considering the Stokesian basis in separable form according to (2.1) with \mathbf{S} being the identity tensor, one can transform (A 1) and (A 2) for $\alpha < \alpha'$ and $\alpha > \alpha'$, respectively:

$$\mathbf{T}(\mathbf{r} - \mathbf{r}') = \sum_{\lambda\mu\sigma s} \sum_{\lambda'\mu'\sigma' s'} C_{\lambda\mu\lambda'\mu'}^{\sigma\sigma'} f_{\lambda\mu\sigma}^+(\alpha) f_{\lambda'\mu'\sigma'}^-(\alpha') \mathbf{e}_{\lambda\mu s}(\beta, \gamma) \mathbf{e}_{\lambda'\mu' s'}(\beta', \gamma') \quad (\text{A } 3)$$

and

$$\mathbf{T}(\mathbf{r} - \mathbf{r}') = \sum_{\lambda\mu\sigma s} \sum_{\lambda'\mu'\sigma' s'} C_{\lambda\mu\lambda'\mu'}^{\sigma\sigma'} f_{\lambda\mu\sigma}^-(\alpha) f_{\lambda'\mu'\sigma'}^+(\alpha') \mathbf{e}_{\lambda\mu s}(\beta, \gamma) \mathbf{e}_{\lambda'\mu' s'}(\beta', \gamma'). \quad (\text{A } 4)$$

We use (A 3) and (A 4) along with a few special properties of the Oseen tensor to simplify the coefficients $C_{\lambda\mu\lambda'\mu'}^{\sigma\sigma'}$. These properties are described next.

A.2. Expansion of Dirac delta function

In order to simplify $C_{\lambda\mu\lambda'\mu'}^{\sigma\sigma'}$, we first consider the Oseen tensor as a Greens function for Stokes equation so that

$$\nabla^2 \mathbf{T}(\mathbf{r} - \mathbf{r}') - \nabla \nabla G_r = \mathbf{I} \delta(\mathbf{r} - \mathbf{r}'). \quad (\text{A } 5)$$

Here, G_r is Greens function of Laplace equation as defined by (3.14), \mathbf{I} is the identity tensor, and $\delta(\mathbf{r} - \mathbf{r}')$ is the Dirac delta function.

In the next step, we expand each term in (A 5) using the outer product of $\mathbf{e}_{\lambda\mu s}(\beta, \gamma)$ and $\mathbf{e}_{\lambda'\mu' s'}(\beta', \gamma')$. We take into account

$$\mathbf{I} \delta(\mathbf{r} - \mathbf{r}') = |\nabla \alpha| |\nabla \beta| |\nabla \gamma| \delta(\alpha - \alpha') \delta(\beta - \beta') \delta(\gamma - \gamma') \mathbf{I} \quad (\text{A } 6)$$

and

$$\delta(\beta - \beta')\delta(\gamma - \gamma')\mathbf{I} = \sum_{\lambda\mu s} \sum_{\lambda'\mu's'} \delta_{\lambda\lambda'}\delta_{\mu\mu'}\delta_{ss'} \mathbf{e}_{\lambda\mu s}(\beta, \gamma) \mathbf{e}_{\lambda'\mu's'}(\beta', \gamma') \quad (\text{A } 7)$$

to conclude

$$\mathbf{I}\delta(\mathbf{r} - \mathbf{r}') = |\nabla\alpha||\nabla\beta||\nabla\gamma| \delta(\alpha - \alpha') \sum_{\lambda\mu s} \sum_{\lambda'\mu's'} \delta_{\lambda\lambda'}\delta_{\mu\mu'}\delta_{ss'} \mathbf{e}_{\lambda\mu s}(\beta, \gamma) \mathbf{e}_{\lambda'\mu's'}(\beta', \gamma'). \quad (\text{A } 8)$$

Moreover, from (3.11) and (3.14), we respectively find for $\alpha < \alpha'$ and $\alpha > \alpha'$

$$\begin{aligned} -\nabla\nabla G_r &= \sum_{\lambda\mu} \mathbf{v}_{\lambda\mu 0}^+(\mathbf{r}) \mathbf{v}_{\lambda\mu 2}^-(\mathbf{r}) d\lambda \\ &= \sum_{\lambda\mu s} \sum_{\lambda'\mu's'} \delta_{\lambda\lambda'}\delta_{\mu\mu'} f_{\lambda\mu s 0}^{+*}(\alpha) f_{\lambda'\mu's 2}^-(\alpha') \mathbf{e}_{\lambda\mu s}(\beta, \gamma) \mathbf{e}_{\lambda'\mu's'}(\beta', \gamma') \end{aligned} \quad (\text{A } 9)$$

and

$$\begin{aligned} -\nabla\nabla G_r &= \sum_{\lambda\mu} \mathbf{v}_{\lambda\mu 2}^-(\mathbf{r}) \mathbf{v}_{\lambda\mu 0}^+(\mathbf{r}) d\lambda \\ &= \sum_{\lambda\mu s} \sum_{\lambda'\mu's'} \delta_{\lambda\lambda'}\delta_{\mu\mu'} f_{\lambda\mu s 2}^{-*}(\alpha) f_{\lambda'\mu's 0}^+(\alpha') \mathbf{e}_{\lambda\mu s}(\beta, \gamma) \mathbf{e}_{\lambda'\mu's'}(\beta', \gamma'). \end{aligned} \quad (\text{A } 10)$$

Also, noting that the separable form of the Stokesian basis solution is associated with a second-order Sturm–Liouville operator, we identify that

$$\nabla^2 \mathbf{T}(\mathbf{r} - \mathbf{r}') = |\nabla\alpha||\nabla\beta||\nabla\gamma| \sum_{\lambda\mu\sigma s} \sum_{\lambda'\mu'\sigma's'} C_{\lambda\mu\lambda'\mu'}^{\sigma\sigma'} \hat{\mathcal{L}}_{\lambda\mu}^{\alpha}(f_{\lambda\mu s\sigma}^{\pm}) f_{\lambda'\mu'\sigma's'}^{\mp}(\alpha') \mathbf{e}_{\lambda\mu s}(\beta, \gamma) \mathbf{e}_{\lambda'\mu'\sigma's'}(\beta', \gamma'), \quad (\text{A } 11)$$

where Sturm–Liouville operator $\hat{\mathcal{L}}_{\lambda\mu}^{\alpha}$ is defined as

$$\hat{\mathcal{L}}_{\lambda\mu}^{\alpha} = S(\alpha) \left[\frac{d}{d\alpha} \left(p(\alpha) \frac{d}{d\alpha} \right) + q_{\lambda\mu}(\alpha) \right], \quad (\text{A } 12)$$

and both cases for $\alpha < \alpha'$ and $\alpha > \alpha'$ are respectively accounted for by reversing the appearance of the superscripts + and – as indicated in (A 3) and (A 4).

After substituting (A 8)–(A 11) in (A 5), we multiply the resulting equation by $|\nabla\alpha||\nabla\beta||\nabla\gamma|$ and integrate it over an infinitely small interval of α around $\alpha = \alpha'$. From the discontinuity at $\alpha = \alpha'$, we find

$$\begin{aligned} \sum_{\lambda\mu\sigma s} \sum_{\lambda'\mu'\sigma's'} C_{\lambda\mu\lambda'\mu'}^{\sigma\sigma'} W(\lambda\mu s\sigma, \lambda'\mu'\sigma's' | \alpha') \mathbf{e}_{\lambda\mu s}(\beta, \gamma) \mathbf{e}_{\lambda'\mu'\sigma's'}(\beta', \gamma') \\ = \sum_{\lambda\mu s} \sum_{\lambda'\mu's'} \delta_{\lambda\lambda'}\delta_{\mu\mu'}\delta_{ss'} \mathbf{e}_{\lambda\mu s}(\beta, \gamma) \mathbf{e}_{\lambda'\mu's'}(\beta', \gamma'), \end{aligned} \quad (\text{A } 13)$$

where, $W(\lambda\mu s\sigma, \lambda'\mu'\sigma's' | \alpha')$ represents a generalized Wronskian

$$W(\lambda\mu s\sigma, \lambda'\mu'\sigma's' | \alpha') = S(\alpha') p(\alpha') \left(f_{\lambda'\mu'\sigma's'}^+ \frac{df_{\lambda\mu s\sigma}^-}{d\alpha'} - f_{\lambda'\mu'\sigma's'}^- \frac{df_{\lambda\mu s\sigma}^+}{d\alpha'} \right). \quad (\text{A } 14)$$

Hence, comparing between two sides of (A 13), we have

$$\sum_{\sigma\sigma'} C_{\lambda\mu\lambda'\mu'}^{\sigma\sigma'} W(\lambda\mu s\sigma, \lambda'\mu'\sigma's' | \alpha') = \delta_{\lambda\lambda'}\delta_{\mu\mu'}\delta_{ss'}. \quad (\text{A } 15)$$

Accordingly, we conclude that

$$C_{\lambda\mu\lambda'\mu'}^{\sigma\sigma'} = \delta_{\lambda\lambda'}\delta_{\mu\mu'}C_{\sigma\sigma'}, \quad (\text{A } 16)$$

which also ensures the disappearance of the α' -dependence on the left-hand side of (A 15) due to the special property of Wronskian.

A.3. Construction of properly normalized stokesian basis

The immediate implication of (A 16) is the simplification of (A 1) and (A 2):

$$\mathbf{T}(\mathbf{r} - \mathbf{r}') = \sum_{\sigma\sigma'} C_{\sigma\sigma'} \mathbf{v}_{\lambda\mu\sigma}^+(\mathbf{r}) \mathbf{v}_{\lambda\mu\sigma'}^-(\mathbf{r}') \quad \text{when } \alpha < \alpha' \quad (\text{A } 17)$$

and

$$\mathbf{T}(\mathbf{r} - \mathbf{r}') = \sum_{\sigma\sigma'} C_{\sigma\sigma'} \mathbf{v}_{\lambda\mu\sigma}^-(\mathbf{r}) \mathbf{v}_{\lambda\mu\sigma'}^+(\mathbf{r}') \quad \text{when } \alpha > \alpha'. \quad (\text{A } 18)$$

However, further simplification of the expansion is possible by using the recurring Curl relation which relates Stokesian solutions with different σ s.

We recognize the tensor $\nabla\nabla'\mathbf{G}_r$ (with ∇' being the gradient in \mathbf{r}' space) as

$$\nabla\nabla'\mathbf{G}_r = \int_{-\infty}^{\infty} \sum_{\mu=-\infty}^{\infty} \mathbf{v}_{\lambda\mu 0}^{+*}(\mathbf{r}') \mathbf{v}_{\lambda\mu 2}^-(\mathbf{r}) d\lambda, \quad (\text{A } 19)$$

and relate it to \mathbf{T} in three equivalent ways

$$\nabla \times \nabla \times \mathbf{T} = -\nabla\nabla'\mathbf{G}_r, \quad \nabla' \times \nabla' \times \mathbf{T} = -\nabla\nabla'\mathbf{G}_r, \quad \nabla \times \nabla' \times \mathbf{T} = \nabla\nabla'\mathbf{G}_r. \quad (\text{A } 20)$$

When (A 17) and (A 18) are substituted in (A 20), and recurring curl relations as described by (3.3) and (3.4) are used with $q^{+*} = q^- = q_1^{+*} = q_1^- = i$, one can find the following relations:

$$C_{00} = C_{11} = C_{22} = 1, \quad C_{01} = C_{02} = C_{12} = 0, \quad C_{10} = C_{21} = k_1, \quad C_{20} = k_2. \quad (\text{A } 21)$$

Here k_1 and k_2 are two arbitrary constants whose values cannot be predicted without a detailed knowledge of the pressure solution. This non-uniqueness stems from the gauge invariant property of the pressure solution.

At this point let us assume that the transformation relations are obtained with specific values of k_1 and k_2 for a certain Stokesian pressure solution $\mathbf{v}_{\lambda\mu 0}^-$ and $\mathbf{v}_{\lambda\mu 2}^+$ which satisfy the recurring curl relations in (3.3) and (3.4) respectively. Then we can conceive of the following gauge transformation where new basis functions corresponding to pressure solutions are constructed using the old basis functions:

$$\mathbf{v}_{\lambda\mu 0}^- + \frac{k_1}{2} \mathbf{v}_{\lambda\mu 1}^- + \frac{k_2 - k_1^2/4}{2} \mathbf{v}_{\lambda\mu 2}^- \rightarrow \mathbf{v}_{\lambda\mu 0}^-, \quad \mathbf{v}_{\lambda\mu 2}^+ + \frac{k_1}{2} \mathbf{v}_{\lambda\mu 1}^+ + \frac{k_2 - k_1^2/4}{2} \mathbf{v}_{\lambda\mu 0}^+ \rightarrow \mathbf{v}_{\lambda\mu 2}^+. \quad (\text{A } 22)$$

and other solutions are obtained by taking successive curl of the new pressure basis. Then, substituting the old basis functions with the new ones in (A 17) and (A 18), one can prove (3.16). In the process, the particular gauge transformation relations in (A 21) render the uniqueness of the Stokesian basis solutions.

Appendix B. Derivation of the transformation coefficients

In this appendix, we derive the expressions for transformation coefficients $T_r(\mathbf{R} | lm0, \lambda\mu 2)$, $T_r(\mathbf{R} | lm1, \lambda\mu 2)$, $T_r(\mathbf{R} | lm2, \lambda\mu 2)$ given in (3.26)–(3.29). According

to our analysis, if these constants are known, we can find all other elements in T_r and T_f by using (3.7)–(3.10), (3.18).

B.1. Transformation relation between two sets of scalar harmonics

Because of our choice of $q^+ = q_1^+$ (both are i), (3.9) ensures

$$T_r(\mathbf{R} | lm2 | \lambda\mu2) = T_r(\mathbf{R} | lm0 | \lambda\mu0). \tag{B 1}$$

Then, according to (3.10), one can write

$$\mathbf{v}_{\lambda\mu0}^+ = \sum_{lm} \mathbf{v}_{lm0}^{1+} T_r(\mathbf{R} | lm0, \lambda\mu0) = \sum_{lm} \mathbf{v}_{lm0}^{1+} T_r(\mathbf{R} | lm2, \lambda\mu2), \tag{B 2}$$

which implies that the potential solution of Stokes equation cannot have any coupling with vorticity and pressure solutions. Considering (3.11), we conclude

$$\Phi_{\lambda\mu}^+ = \sum_{lm} \Phi_{lm}^{1+} T_r(\mathbf{R} | lm0, \lambda\mu0). \tag{B 3}$$

In our analysis, $T_r(\mathbf{R} | lm2 | \lambda\mu2)$ is obtained by relating the scalar harmonic functions $\Phi_{\lambda\mu}^+$ and Φ_{lm}^{1+} defined in (3.12).

By using properties of the modified Bessel function $I_\mu(\lambda\rho)$, $\Phi_{\lambda\mu}^+$ can be expanded as

$$\Phi_{\lambda\mu}^+ = \frac{1}{4\pi^2} \int_0^{2\pi} \exp[\lambda\rho \cos(\beta - \psi) + i\mu\psi + i\lambda z] d\psi. \tag{B 4}$$

If cylinder centre and sphere centre are separated by $\mathbf{R} = R\mathbf{e}_x$, then from the geometry one finds

$$\rho \cos(\beta - \psi) = r \sin(\theta) \cos(\phi - \psi) + R \cos(\psi), \quad z = r \cos(\theta). \tag{B 5}$$

Substituting (B 5) in (B 4), we get

$$\Phi_{\lambda\mu}^+ = \frac{1}{4\pi^2} \int_0^{2\pi} \exp[\lambda r \sin(\theta) \cos(\phi - \psi) + i\lambda r \cos(\theta) + \lambda R \cos(\psi) + i\mu\psi] d\psi. \tag{B 6}$$

On the other hand, Taylor series expansion shows

$$\exp[\lambda r \sin(\theta) \cos(\phi - \psi) + i\lambda r \cos(\theta)] = \sum_{l=1}^{\infty} \sum_{m=-l}^l 4\sqrt{\pi} C_{lm} (i\lambda)^l (i^m) e^{-im\psi} \Phi_{lm}^{1+}, \tag{B 7}$$

where C_{lm} is defined in (3.29). Hence substituting (B 7) in (B 6) and using properties of modified Bessel function $I_\mu(\lambda\rho)$, the following expression can be obtained

$$\Phi_{\lambda\mu}^+ = \sum_{l=1}^{\infty} \sum_{m=-l}^l M(\lambda, \mu; l, m) C_{lm} \Phi_{lm}^{1+}, \tag{B 8}$$

where $M(\lambda, \mu; l, m)$ is given in (3.29). So finally we prove

$$T_r(lm0, \lambda\mu0) = T_r(lm2, \lambda\mu2) = M(\lambda, \mu; l, m) C_{lm} \tag{B 9}$$

by comparing (B 3) and (B 8). The expression in (B 9) is same as the one given in (3.26).

B.2. Expansion of cylindrical pressure solution

In order to find the other two independent transformation coefficients ($T_r(\mathbf{R} | lm0, \lambda\mu2)$ and $T_r(\mathbf{R} | lm1, \lambda\mu2)$), we express $\mathbf{v}_{\lambda\mu2}^+$ in terms of the potential solution. We construct

a linear tensorial operator \mathbf{L}_λ which relates $\mathbf{v}_{\lambda\mu 2}^+$ in terms of $\mathbf{v}_{\lambda\mu 0}^+$

$$\mathbf{v}_{\lambda\mu 2}^+ = \mathbf{L}_\lambda \cdot \mathbf{v}_{\lambda\mu 0}^+, \quad (\text{B } 10)$$

where

$$\mathbf{L}_\lambda = \frac{1}{2\lambda^2} \left(\rho \frac{\partial}{\partial \rho} \mathbf{I} + \mathbf{e}_z \mathbf{e}_z \right). \quad (\text{B } 11)$$

It is to be noted that (B 10) is a reverse relation for the recurrence Curl structure in (3.4). In (3.4), $\mathbf{v}_{\lambda\mu 0}^+$ can be determined if $\mathbf{v}_{\lambda\mu 2}^+$ is given whereas in (B 10) the reverse is true. We often refer to operators like \mathbf{L}_λ as reverse curl operators for the particular basis vectors.

As the operator \mathbf{L}_λ is linear, it can operate on the expansion in (B 2) so that

$$\mathbf{v}_{\lambda\mu 2}^+ = \mathbf{L}_\lambda \cdot \mathbf{v}_{\lambda\mu 0}^+ = \sum_{lm} \mathbf{u}_{lm}^{\lambda 1+} T_r(\mathbf{R} | lm2, \lambda\mu 2), \quad (\text{B } 12)$$

where

$$\mathbf{u}_{lm}^{\lambda 1+} = \mathbf{L}_\lambda \cdot \mathbf{v}_{lm0}^{1+}. \quad (\text{B } 13)$$

We express $\mathbf{u}_{lm}^{\lambda 1+}$ in terms of spherical basis solutions by using the following identity which is derived in our analysis

$$\mathbf{u}_{lm}^{\lambda 1+} = a_{lm\lambda} \mathbf{v}_{l-2m0}^{1+} + b_{lm\lambda} \mathbf{v}_{l-1m1}^{1+} + c_{lm\lambda} \mathbf{v}_{lm2}^{1+} + c_{lm\lambda}^+ \mathbf{v}_{l-1m+10}^{1+} - c_{lm\lambda}^- \mathbf{v}_{l-1m-10}^{1+}. \quad (\text{B } 14)$$

Hence after replacing $T_r(\mathbf{R} | lm2, \lambda\mu 2)$ in (B 12) according to (B 9), $\mathbf{v}_{\lambda\mu 2}^+$ can be expanded as

$$\mathbf{v}_{\lambda\mu 2}^+ = \sum_{lm} M(\lambda, \mu; l, m) C_{lm} (a_{lm\lambda} \mathbf{v}_{l-2m0}^{1+} + b_{lm\lambda} \mathbf{v}_{l-1m1}^{1+} + c_{lm\lambda} \mathbf{v}_{lm2}^{1+} + c_{lm\lambda}^+ \mathbf{v}_{l-1m+10}^{1+} - c_{lm\lambda}^- \mathbf{v}_{l-1m-10}^{1+}). \quad (\text{B } 15)$$

Here the constants $a_{lm\lambda}$, $b_{lm\lambda}$, $c_{lm\lambda}$, $c_{lm\lambda}^+$, $c_{lm\lambda}^-$ are

$$a_{lm\lambda} = -\frac{\sqrt{(l-m)(l-m-1)(l+m)(l+m-1)}}{\lambda^2}, \quad (\text{B } 16)$$

$$b_{lm\lambda} = -\frac{m\sqrt{(l-m)(l+m)}}{\lambda^2}, \quad (\text{B } 17)$$

$$c_{lm\lambda} = \frac{l(l-1)(2l-1) - (l^2 - m^2)(l-2)}{2l(2l-1)\lambda^2}, \quad (\text{B } 18)$$

$$c_{lm\lambda}^+ = \frac{R\sqrt{(2l+1)(l-m-1)(l-m)}}{4\lambda^2\sqrt{(2l-1)}}, \quad (\text{B } 19)$$

$$c_{lm\lambda}^- = -\frac{R\sqrt{(2l+1)(l+m-1)(l+m)}}{4\lambda^2\sqrt{(2l-1)}}. \quad (\text{B } 20)$$

Substituting (B 16)–(B 20) in (B 15), all independent transformation coefficients can be evaluated.

The final forms can be significantly simplified if one considers the following identities involving the constants $a_{lm\lambda}$, $b_{lm\lambda}$, $c_{lm\lambda}$, $c_{lm\lambda}^+$, $c_{lm\lambda}^-$:

$$a_{lm\lambda} M(\lambda, \mu; l, m) C_{lm} = M(\lambda, \mu; l-2, m) C_{l-2m}, \quad (\text{B } 21)$$

$$b_{lm\lambda} M(\lambda, \mu; l, m) C_{lm} = -\frac{im}{\lambda} M(\lambda, \mu; l-1, m) C_{l-1m}, \quad (\text{B } 22)$$

$$c_{lm\lambda}M(\lambda, \mu; l, m)C_{lm} = \frac{l(l-1)(2l-1) - (l^2 - m^2)(l-2)}{2l(2l-1)\lambda^2}M(\lambda, \mu; l, m)C_{lm}, \quad (\text{B } 23)$$

$$c_{lm\lambda}^+M(\lambda, \mu; l, m)C_{lm} = \frac{R}{4\lambda^2}M(\lambda, \mu; l, m)C_{l-1m+1}, \quad (\text{B } 24)$$

$$c_{lm\lambda}^-M(\lambda, \mu; l, m)C_{lm} = \frac{R}{4\lambda^2}M(\lambda, \mu; l, m)C_{l-1m-1}. \quad (\text{B } 25)$$

Then substituting the identities given by (B 21)–(B 25) in (B 15) and changing relevant orders of the summation we find

$$\begin{aligned} \mathbf{v}_{\lambda\mu 2}^+ &= \sum_{lm} c_{lm}M(\lambda, \mu; l, m) \left(\mathbf{v}_{lm2}^{1+} - \frac{im}{\lambda l} \mathbf{v}_{lm1}^{1+} + \frac{l(l-1)(2l-1) - (l^2 - m^2)(l-2)}{2l(2l-1)\lambda^2} \mathbf{v}_{lm0}^{1+} \right) \\ &+ \sum_{lm} c_{lm}(M(\lambda, \mu; l+1, m-1) - M(\lambda, \mu; l+1, m+1))\mathbf{v}_{lm0}^{1+}. \end{aligned} \quad (\text{B } 26)$$

However, we also know that

$$\mathbf{v}_{\lambda\mu 2}^+ = \sum_{lm\sigma} \mathbf{v}_{lm\sigma}^{1+} T_r(\mathbf{R} | lm\sigma, \lambda\mu 2). \quad (\text{B } 27)$$

Hence comparing (B 26) and (B 27) we determine $T_r(\mathbf{R} | lm1, \lambda\mu 2)$ and $T_r(\mathbf{R} | lm0, \lambda\mu 2)$. The expressions are identical to (3.27) and (3.28), respectively.

REFERENCES

- BHATTACHARYA, S. 2008*a* Cooperative motion of spheres arranged in periodic grids between two parallel walls. *J. Chem. Phys.* **128**, 074709.
- BHATTACHARYA, S. 2008*b* History force on an asymmetrically rotating body in Poiseuille flow inducing particle-migration across a slit-pore. *Phys. Fluids* **20**, 093301.
- BHATTACHARYA, S. & BŁAWZDZIEWICZ, J. 2002 Image system for Stokes-flow singularity between two parallel planar walls. *J. Math. Phys.* **43**, 5720–5731.
- BHATTACHARYA, S., BŁAWZDZIEWICZ, J. & WAJNRYB, E. 2005*a* Hydrodynamic interactions of spherical particles in suspensions confined between two planar walls. *J. Fluid Mech.* **541**, 263–292.
- BHATTACHARYA, S., BŁAWZDZIEWICZ, J. & WAJNRYB, E. 2005*b* Many-particle hydrodynamic interactions in parallel-wall geometry: Cartesian-representation method. *Physica A* **356**, 294–340.
- BHATTACHARYA, S., BŁAWZDZIEWICZ, J. & WAJNRYB, E. 2006*a* Far-field approximation for hydrodynamic interactions in parallel-wall geometry. *J. Comput. Phys.* **212**, 718–738.
- BHATTACHARYA, S., BŁAWZDZIEWICZ, J. & WAJNRYB, E. 2006*b* Hydrodynamic interactions of spherical particles in Poiseuille flow between two parallel walls. *Phys. Fluids* **18** (5).
- BRENNER, H. 1970 Pressure drop due to the motion of neutrally buoyant particles in duct flows. *J. Fluid Mech.* **43**, 641–660.
- BRENNER, H. & HAPPEL, J. 1958 Slow viscous flow past a sphere in a cylindrical tube. *J. Fluid Mech.* **4**, 195–213.
- BUNGAY, P. M. & BRENNER, H. 1973*a* Pressure drop due to the motion of a sphere near the wall bounding a Poiseuille flow. *J. Fluid Mech.* **60**, 81–96.
- BUNGAY, P. M. & BRENNER, H. 1973*b* The motion of a closely-fitting sphere in a fluid-filled tube. *Intl J. Multiph. Flow* **1**, 25–56.
- CHIU, J. J., WANG, D. L., CHIEN, S., SKALAK, R. & USAMI, S. 1998 Effects of disturbed flow on endothelial cells. *J. Biomech. Engng – Trans. ASME* **120**, 2–8.
- CICHOCKI, B. & JONES, R. B. 1998 Image representation of a spherical particle near a hard wall. *Physica A* **258**, 273–302.

- CICHOCKI, B., JONES, R. B., KUTTEH, R. & WAJNRYB, E. 2000 Friction and mobility for colloidal spheres in Stokes flow near a boundary: the multipole method and applications. *J. Chem. Phys.* **112**, 2548–61.
- COX, R. G. & BRENNER, H. 1967 Effect of finite boundaries on Stokes resistance of an arbitrary particle. 3. Translation and rotation. *J. Fluid Mech.* **28**, 391.
- COX, R. G. & MASON, S. G. 1971 Suspended particles in fluid flow through tubes. *Annu. Rev. Fluid Mech.* **3**, 291–316.
- DRAZER, G., KHUSID, B., KOPLIK, J. & ACRIVOS, A. 2005 Wetting and particle adsorption in nanoflows. *Phys. Fluids* **17**, ARTN:017102.
- DURLOFSKY, L. J. & BRADY, J. F. 1989 Dynamic simulation of bounded suspensions of hydrodynamically interacting particles. *J. Fluid Mech.* **200**, 39–67.
- DURLOFSKY, L., BRADY, J. F. & BOSSIS, G. 1987 Dynamic simulation of hydrodynamically interacting particles. *J. Fluid Mech.* **180**, 21–49.
- FALADE, A. & BRENNER, H. 1985 Stokes wall effects for particles moving near cylindrical boundaries. *J. Fluid Mech.* **154**, 145–162.
- FELDERHOF, B. U. & JONES, R. B. 1989 Displacement theorems for spherical solutions of the linear Navier–Stokes equations. *J. Math. Phys.* **30**, 339–42.
- GOLDMAN, A. J., COX, R. G. & BRENNER, H. 1967 Slow viscous motion of a sphere parallel to a plane wall – I. Motion through a quiescent fluid. *Chem. Engng Sci.* **22**, 637–651.
- GREENSTEIN, T. & HAPPEL, J. 1968 Theoretical study of the slow motion of a sphere and a fluid in a cylindrical tube. *J. Fluid Mech.* **34**, 705–710.
- GREENSTEIN, T. & HAPPEL, J. 1970 Viscosity of dilute uniform suspensions of sphere spheres. *Phys. Fluids* **13**, 18–21.
- HIGDON, J. J. L. & MULDOWNY, G. P. 1995 Resistance functions for spherical particles, droplets and bubbles in cylindrical tubes. *J. Fluid Mech.* **298**, 193–210.
- LADD, A. J. C. 1988 Hydrodynamic interactions in suspensions of spherical particles. *J. Chem. Phys.* **88**, 5051.
- LAMB, H. 1945 *Hydrodynamics*. Dover.
- LUNSMANN, W. J., GENIESER, L., ARMSTRONG, R. C. & BROWN, R. A. 1993 Finite-element analysis of steady viscoelastic flow around a sphere in a tube-calculations with constant viscosity models. *J. Non-Newton. Fluid Mech.* **48**, 63–99.
- MORRIS, J. F. & BRADY, J. F. 1998 Pressure-driven flow of a suspension: buoyancy effects. *Intl J. Multiph. Flow* **24**, 105–30.
- NOTT, P. R. & BRADY, J. F. 1994 Pressure-driven flow of suspensions – simulation and theory. *J. Fluid Mech.* **275**, 157–199.
- O'NEILL, M. E. & STEWARTSON, K. 1967 On the slow motion of a sphere parallel to a nearby plane wall. *J. Fluid Mech.* **27**, 705–724.
- POZRIKIDIS, C. 2005 Numerical simulation of cell motion in tube flow. *Ann. Biomed. Engng* **33**, 165–178.
- QUEGUINER, C. & BARTHESBIESEL, D. 1997 Axisymmetric motion of capsules through cylindrical channels. *J. Fluid Mech.* **348**, 349–376.
- SIEROU, A. & BRADY, J. F. 2001 Accelerated Stokesian dynamics simulations. *J. Fluid Mech.* **448**, 115–46.
- SUGIHARASEKI, M. 1996 The motion of an ellipsoid in tube flow at low Reynolds numbers. *J. Fluid Mech.* **324**, 287–308.
- SUGIHARASEKI, M. & SKALAK, R. 1997 Asymmetric flows of spherical particles in a cylindrical tube. *Biorheology* **34**, 155–169.
- SUSHKO, N. & CIEPLAK, M. 2001 Motion of grains, droplets, and bubbles in fluid-filled nanopores. *Phys. Rev. E* **64**.
- TOZEREN, H. 1982 Torque on eccentric spheres flowing in tubes. *J. Appl. Mech. Trans. ASME* **49**, 279–283.
- TOZEREN, H. 1983 Drag on eccentrically positioned spheres translating and rotating in tubes. *J. Fluid Mech.* **129**, 77–90.
- WANG, H. & SKALAK, R. 1969 Viscous flow in a cylindrical tube containing a line of spherical particles. *J. Fluid Mech.* **38**, 75–96.